

2024-05-01

Investigating changes in surface water chemistry across the Llano Uplift and the Balcones fault zone in central Texas using strontium and uranium isotopes

Hao Tuan Pham
University of Texas at El Paso

Follow this and additional works at: https://scholarworks.utep.edu/open_etd



Part of the [Environmental Sciences Commons](#), [Geochemistry Commons](#), and the [Geology Commons](#)

Recommended Citation

Pham, Hao Tuan, "Investigating changes in surface water chemistry across the Llano Uplift and the Balcones fault zone in central Texas using strontium and uranium isotopes" (2024). *Open Access Theses & Dissertations*. 4134.

https://scholarworks.utep.edu/open_etd/4134

This is brought to you for free and open access by ScholarWorks@UTEP. It has been accepted for inclusion in Open Access Theses & Dissertations by an authorized administrator of ScholarWorks@UTEP. For more information, please contact lweber@utep.edu.

INVESTIGATING CHANGES IN SURFACE WATER CHEMISTRY ACROSS
THE LLANO UPLIFT AND THE BALCONES FAULT ZONE IN CENTRAL
TEXAS USING STRONTIUM AND URANIUM ISOTOPES

HAO TUAN PHAM

Master's Program in Geological Sciences

APPROVED:

Jason Ricketts, Ph.D., Chair

Lin Ma, Ph.D., Co-Chair

Victor Garcia, Ph.D.

Stephen L. Crites, Jr., Ph.D.

Dean of the Graduate School

Copyright
by
Hao Tuan Pham
2024

INVESTIGATING CHANGES IN SURFACE WATER CHEMISTRY ACROSS
THE LLANO UPLIFT AND THE BALCONES FAULT ZONE IN CENTRAL
TEXAS USING STRONTIUM AND URANIUM ISOTOPES

by

HAO TUAN PHAM, B.S.

THESIS

Presented to the Faculty of the Graduate School of

The University of Texas at El Paso

in Partial Fulfillment

of the Requirements

for the Degree of

MASTER OF SCIENCE

Department of Earth, Environmental, and Resource Sciences

THE UNIVERSITY OF TEXAS AT EL PASO

May 2024

ACKNOWLEDGEMENTS

I would like to give many thanks to the people, friends, and mentors who assisted me over the last 6 years here at UTEP. Special thanks to Nuria who spent many hours and many days with me collecting and analyzing my strontium samples, Jennifer who helped me with the uranium samples, Alan who is a great field assistant, Victor thank you for introducing me to this wonderful project, JEM group who has given me insightful feedback on my presentations, Dr. Jason Ricketts who has been a tremendous mentor throughout the years, Dr. Lin Ma with his fantastic guidance, and lastly, I would like to give a special thanks to Walter Vernon Kramer, an amazing teacher and mining geologist, without him, I wouldn't be where I am today.

From the depth of my heart, thank you everyone for continuing to believe in me and your unwavering support.

ABSTRACT

The landscape of central Texas is shaped by over one billion years of Earth's history. An array of lithology lies within central Texas along with two large geological structures. The Llano Uplift, characterized by Proterozoic metamorphic and igneous rocks dating back to 1.37 billion years ago, is encircled by Paleozoic and Mesozoic sedimentary rocks. To the southeast of the Llano Uplift lies the Balcones Fault Zone (BFZ), an extensional structural system of mostly normal faults that delineates the transition between Paleozoic-Mesozoic sedimentary rocks and Cenozoic sedimentary cover, which are influential to the regional hydrogeology. This study investigates the hydrogeological dynamics influenced by these geological features, focusing on spatial variations in surface water chemistry across these two features. In this region, rivers traversing through Paleozoic-Mesozoic carbonate rocks exhibit elevated electrical conductivity (EC) and bicarbonate (HCO_3) concentrations due to chemical weathering processes, while those flowing over Proterozoic crystalline rocks demonstrate lower EC levels. This study also reveals significant trends in strontium and uranium isotopic ratios, providing insights into water-rock interactions and potential groundwater influences in the BFZ and the Llano Uplift. These insights advance our understanding and knowledge of the hydrogeological processes and implications for water resource management, groundwater sustainability, and contamination mitigation efforts in central Texas.

TABLE OF CONTENTS

ACKNOWLEDGEMENTS	iv
ABSTRACT	v
TABLE OF CONTENTS	vi
LIST OF TABLES	viii
LIST OF FIGURES	ix
CHAPTER 1: INTRODUCTION	1
1.1. Motivation	1
CHAPTER 2: GEOLOGICAL AND HYDROGEOLOGICAL SETTINGS	2
2.1. Llano Uplift	3
2.2. Balcones Fault Zone	4
2.3. Mesozoic and Cenozoic Sedimentary Cover	5
2.4. Major aquifers and river systems in the study area	5
CHAPTER 3: STRONTIUM AND URANIUM ISOTOPE GEOCHEMISTRY	9
3.1. Strontium Isotopes	9
3.2. Uranium Isotopes	11
CHAPTER 4: METHODS	13
4.1. Sample Collection	13
4.2. Sample Preparation for Geochemical Analysis: major elements, ($^{87}\text{Sr}/^{86}\text{Sr}$) and ($^{234}\text{U}/^{238}\text{U}$) ratios	15
4.2.1. <i>Major and trace elements</i>	15
4.2.2. $^{87}\text{Sr}/^{86}\text{Sr}$ Analysis	16
4.2.3. $^{234}\text{U}/^{238}\text{U}$ Analysis	17
4.3. GIS and Geological Data Integration and Analysis	17
CHAPTER 5: RESULTS	19
5.1. Schematic Cross-Section	19
5.2. Electrical Conductivity	23
5.3. Bicarbonate (HCO_3)	24
5.4. $^{87}\text{Sr}/^{86}\text{Sr}$ Results	26
5.5. $^{234}\text{U}/^{238}\text{U}$ Results	28
5.6. Geochemical Trends	30
5.6.1. <i>Trends in Electrical Conductivity (EC)</i>	30

5.6.2. <i>Trends in Bicarbonate (HCO₃)</i>	32
5.6.3. <i>Trends in Major Elements</i>	34
5.7. <i>Trends in Sr and U isotope vs. concentrations</i>	35
CHAPTER 6: DISCUSSIONS	38
6.1. Endmember Lithologies Affect Downstream River Chemistry.....	38
6.2. Bicarbonate (HCO ₃)	40
6.3. Lithologic Controls on Sr and U	41
6.4. Vertical and Structural Controls on Electrical Conductivity	43
6.5. The Influence of Geologic Structure on River Chemistry	45
6.5.1. Llano Uplift.....	46
6.5.2. Balcones Fault Zone	47
6.6. Schematic conceptual model of surface water chemistry changes in Central Texas.....	48
CHAPTER 7: CONCLUSION	51
REFERENCES	52
VITA	60

LIST OF TABLES

Table 1: Generalized U isotope ratios in different water type and Sr isotopes ratios in different lithology across central Texas.....	12
Table 2. River Samples and Springs data	21
Table 3. Major Elements (ppm)	22
Table 4. Sr Isotope Data.....	25
Table 5. U Isotope Data	28

LIST OF FIGURES

Figure 1: (A) Simplified geologic map with rock types, faults, rivers, and water of the study area. (B) Geologic map of Texas from Texas Almanac n.d. (C) And modified Balcones fault zone map. Red box is the study area.	2
Figure 2: Edwards and Trinity aquifers map with Llano Uplift and BFZ region with rivers, springs, and city.	6
Figure 3: Modified cross-section figure by Texas State University modified from Barker and Ardis (1996) and Lindgren and others (2004). Trinity and Edwards aquifers cross section with different lithologies and structure.	7
Figure 4: Modified diagram from Bataille & Bowen (2012) displaying Sr isotopes ratios for major bedrock lithologies in the United States; (A) $^{87}\text{Sr}/^{86}\text{Sr}$ variations from bedrock models; (B) $^{87}\text{Sr}/^{86}\text{Sr}$ variations from bedrock age-only model.	10
Figure 5: Sample map of the study area. Geology is the same as Fig.1A. LU - Llano Uplift; LU-BFZ – Llano Uplift to Balcones fault zone; BFZ – Balcones fault zone.	13
Figure 6: A-A' (A) Geologic map with rock units, rivers, and faults, showing the location of the cross-section. (B) Schematic cross-section of the study area highlighting major rock types and structures.	20
Figure 7: Electrical conductivity (EC) of samples collected in this study. Samples are grouped by location (different symbols) and color-coded by EC value.	23
Figure 8: Bicarbonate (HCO_3) samples collected in this study. Samples are grouped by location (different symbols) and color-coded by HCO_3 value.	24
Figure 9: $^{87}\text{Sr}/^{86}\text{Sr}$ ratios of samples collected in this study. Samples are grouped by location (different symbols) and color-coded by Sr ratio.	26

Figure 10: $^{234}\text{U}/^{238}\text{U}$ ratios of samples collected in this study. Samples are grouped by location (different symbols) and color-coded by U ratio..... 29

Figure 11: (A) EC (us/cm) vs Sr (ppm) and (B) U (ppb) plots with different sample types. Llano Uplift (orange circle), in-between LU and BFZ (purple diamond), Balcones fault zone (blue square), and springs (green triangle)..... 31

Figure 12: (A) Sr and (B) U vs HCO_3 plots with different sample types. Llano Uplift (orange circle), in-between LU and BFZ (purple diamond), Balcones fault zone (blue square), and springs (green triangle). 33

Figure 13: Major element ratio plot with different sample types. Llano Uplift (orange circle), in-between LU and BFZ (purple diamond), Balcones fault zone (blue square), and springs (green triangle). 34

Figure 14: (A) Sr ratio vs Sr (ppm) and (B) U ratio vs U (ppb) plots. Llano Uplift (orange circle), in-between LU and BFZ (purple diamond), Balcones fault zone (blue square), and springs (green triangle). 35

Figure 15: Sr vs U ratio plot with different sample types. Llano Uplift (orange circle), in-between LU and BFZ (purple diamond), Balcones fault zone (blue square), and springs (green triangle).36

Figure 16: Mixing diagrams using Na-normalized molar ratio element in the study area plotted with 60 largest rivers from Gaillardet et al., (1999) with rivers having TDS values greater than 500 mg l⁻¹ (open circles). Study area samples are modified to prior to LU (light blue circle), within the LU (dark blue circle), in-between LU and BFZ (dark green circle), within the BFZ (light green circle), after BFZ (brown circle), and springs (triangle). 39

Figure 17: Modified table from Maclay and Small (1984) summary of the lithology and water-bearing characteristic on the San Marcos Platform in the Balcones fault zone..... 44

Figure 18: Plot total dissolved solids (TDS) in mg/L vs distance of the Llano Uplift (blue region) and Balcones fault zone (green region). 45

Figure 19: Plot of Sr and U ratio vs distance of the Llano Uplift (blue region) and Balcones fault zone (green region). 45

Figure 20: Cross-sectional schematic model illustrating the influence of lithology and structure on surface water chemistry. 49

CHAPTER 1: INTRODUCTION

1.1. Motivation

The hydrogeological dynamics of central Texas are shaped by a myriad of factors such as large geological structures and lithological compositions. The Llano Uplift and the Balcones fault zone (BFZ) stand out as prominent features, potentially exerting influences on surface water chemistry in central Texas. More than 1.7 million people rely on freshwater from aquifers and surface water in central Texas. Therefore, it is crucial to understand these potential influences to effectively apply water resource management, groundwater sustainability, and contamination mitigation efforts. This study delves into the complex interactions between large geological structures, lithology, and surface water chemistry, aiming to provide valuable insights into the hydrogeological dynamics of central Texas. By examining how surface water chemistry changes as rivers flow through different lithologies and structures, this study seeks to highlight the mechanisms driving these variations and their implications for water resource management. Through comprehensive analysis and interpretation of strontium and uranium isotopes and water chemistry parameters in rivers, streams, and springs in this region, this study aims to contribute to a deeper understanding of the complex hydrogeological processes at play in central Texas, with implications extending beyond the region to inform broader water management strategies and environmental protection efforts. This study also highlights the important geologic controls on surface water chemistry.

CHAPTER 2: GEOLOGICAL AND HYDROGEOLOGICAL SETTINGS

Texas possesses a vast geological history that spans over one billion years of Earth's history. The oldest rocks in Texas are primarily located in the central region known as the Llano Uplift. This area consists of deformed Proterozoic rocks that include metasedimentary, metavolcanic, and metaplutonic assemblages that date back to approximately 1.37 - 1.23 Ga (Mosher, 1998). Moreover, post-tectonic granites intruded into this region around 1.13 Ga which caused additional deformation and metamorphism (e.g. Walker, 1992; Mosher,

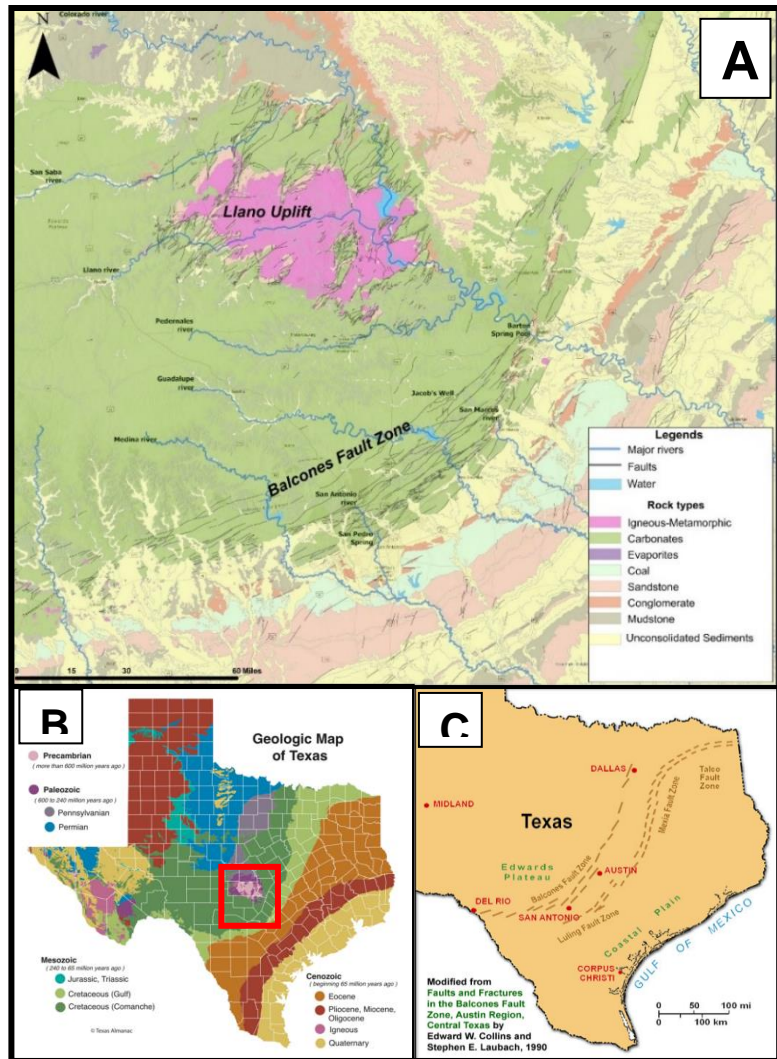


Figure 1: (A) Simplified geologic map with rock types, faults, rivers, and water of the study area. (B) Geologic map of Texas from Texas Almanac n.d. (C) And modified Balcones fault zone map. Red box is the study area.

1998). These Proterozoic rocks are prominently exposed in a circular uplift, encircled by Paleozoic and Cretaceous sedimentary formations (Fig. 1B). The Llano Uplift constitutes the most extensive exposure of Precambrian rocks within the state of Texas. To the east of the Llano Uplift lies a region of Mesozoic and Cenozoic sedimentary rocks, characterized by a gentle southeastward dip towards the Gulf Coast (Collins, 1993). A separation between the Paleozoic-

Mesozoic and Cenozoic sedimentary rocks is marked by the Balcones fault zone (Fig. 1B and 1C). The Balcones fault zone (BFZ) is characterized by a series of en-echelon normal faults trending northeast-southwest from Texarkana to Del Rio, TX (Collins, 1993). This fault zone separates Texas into two distinct regions with differing topographic profiles: the Edwards Plateau, characterized by high elevations to the west, and the Coastal Plains, featuring lower topography to the east (Fig. 1C). Together, the Llano Uplift and the BFZ are integral geological components that shaped the contemporary landscape of present-day Texas. Below I present more detailed descriptions of these two geologic structures.

2.1. Llano Uplift

The Llano Uplift is a gentle structural dome comprised of Middle Proterozoic igneous and metamorphic rocks. Up to 9,000 km² are exposed through an erosional window of Paleozoic and Mesozoic sedimentary rocks (Muehlberger et al., 1967; Flawn and Muehlberger, 1970; Walker, 1992). The most notable of these Proterozoic rocks are the Big Branch Gneiss, Packsaddle Schists, Lost Greek Gneiss, Valley Spring Gneiss, and the Town Mountain Granite. These Proterozoic rocks were subjugated to multiple deformations concurrently with regional metamorphism characterized by moderate- to high-pressure that include upper amphibolite to lower granulite facies (Walker, 1992; Mosher, 1993; Reese, 1995; Roback, 1996; Carlson, 1998). The formation and deformation of these Proterozoic rocks including the post-tectonic plutons, sills, and dikes occurred during the Grenville orogenic event of eastern North America around 1.37-1.05 Ga (Mosher, 1993; Mosher, 1998). The Grenville orogenic event is classified as a northeast-trending continental-continental collision between Laurentia and another continent, contributing to the formation of the early Neoproterozoic supercontinent Rodinia (Davidson, 1986; Rivers et al., 1989; Hynes & Rivers, 2010). Additional deformation of the Llano Uplift

occurred during the Ouachita orogeny around 300 Ma resulting in normal and oblique-slip faults affecting most of the Proterozoic and Pennsylvanian rocks, and which juxtaposed Paleozoic rocks against Proterozoic rocks (Walker, 1992).

2.2. Balcones Fault Zone

The BFZ is an extensional structural system consisting of normal faults, en-echelon faults, cross faults, step faults, grabens, and horsts (Abbott & Woodruff, 1986; Collins, 1993). The fault system ranges between 10 to 60 km wide with a maximum displacement of 366 m (Weeks, 1945). This fault systems may have originated 300 Ma and be related to the Ouachita fault systems that include thrust faults, glide planes, and deep normal fault that follows the trend of the buried Paleozoic Ouachita fold and thrust belt (Flawn et al., 1961; Collins, 1993; Ewing, 2005). These structures may have been reactivated or overprinted in the Oligocene-Miocene to form the BFZ as a response to the receding of the Gulf of Mexico, and it marks the shift from the structurally stable rocks of the Texas craton to the gently southeast coastal-dipping sedimentary deposits of the Gulf of Mexico (Murray, 1961; Rose, 1972; Collins & Hovorka, 1997; Ferrill et al., 2019). In addition, Weeks (1945) proposed that the most recent movement of the Balcones fault zone presumably occurred in the early Neogene from examining the intermixing and interbedding of Cretaceous lithology and fossils with the lower Tertiary Catahoula and Oakville Formations. The intermix of Cretaceous and Tertiary rocks indicates that considerable fault movement had occurred in the early Neogene. Although these faults only have a lesser offset in early Neogene, they are long-lived structures that have been repeatedly reactivated over geologic time. Consequently, they are likely to intersect the Proterozoic basement and can potentially act as conduits for fluid migration. Furthermore, as highlighted by Schindel (2019), the BFZ stands out as a prevalent structural feature controlling the hydrogeology of central-eastern Texas.

2.3. Mesozoic and Cenozoic Sedimentary Cover

Most of central and southern Texas is covered by sedimentary rocks (Fig. 1B). Beginning from central Texas, the predominant rocks consist of Mesozoic carbonate deposits, notably the Glen Rose Formation, which has a thickness of 900 ft. This formation comprises limestone, marl, and dolomite with some zones of evaporites. The Edward Limestone or Edwards Group has a thickness ranging from 300 to 500 ft. and consists of fine- to coarse- grained limestone, grainstone, dolomite, and evaporites. These two dominant formations are Lower Cretaceous in age. Transitioning away from the Mesozoic carbonates, the Cenozoic deposits of southern Texas primarily consist of silicate deposits such as sandstone, mudstone, conglomerates, clay, and to some extent lignite and coal. These Cenozoic deposits are subsequently overlain by a blanket of unconsolidated sediments across southern Texas. Altogether, these sedimentary rocks provide a diverse array of lithology to study the impact of water rock influences.

2.4. Major aquifers and river systems in the study area

The general climate in the study area is classified as sub-tropical and subhumid, characterized by long hot summers, short mild winters, and warm spring according to the Koppen Climate Classification. The region typically experiences an annual temperature range from a high of 80 °F (27 °C) to a low of 56 °F (13 °C), with annual precipitation ranging from 30-40 inches per year (76-102 cm/yr).

The Edwards and Trinity Aquifers are the main sources of freshwater for the majority of the population in south-central Texas (Fig. 2). These aquifers supply fresh water to over 1.7 million people, as well as to industries, agriculture, and recreational activities in the cities of San Antonio and Austin as well as many communities in the Texas Hill Country (Ferrill et al., 2008). The Edwards and Trinity Aquifers are formed from complex karst limestone systems that have permeability features (see Fig. 3) that include a combination of host rock permeability,

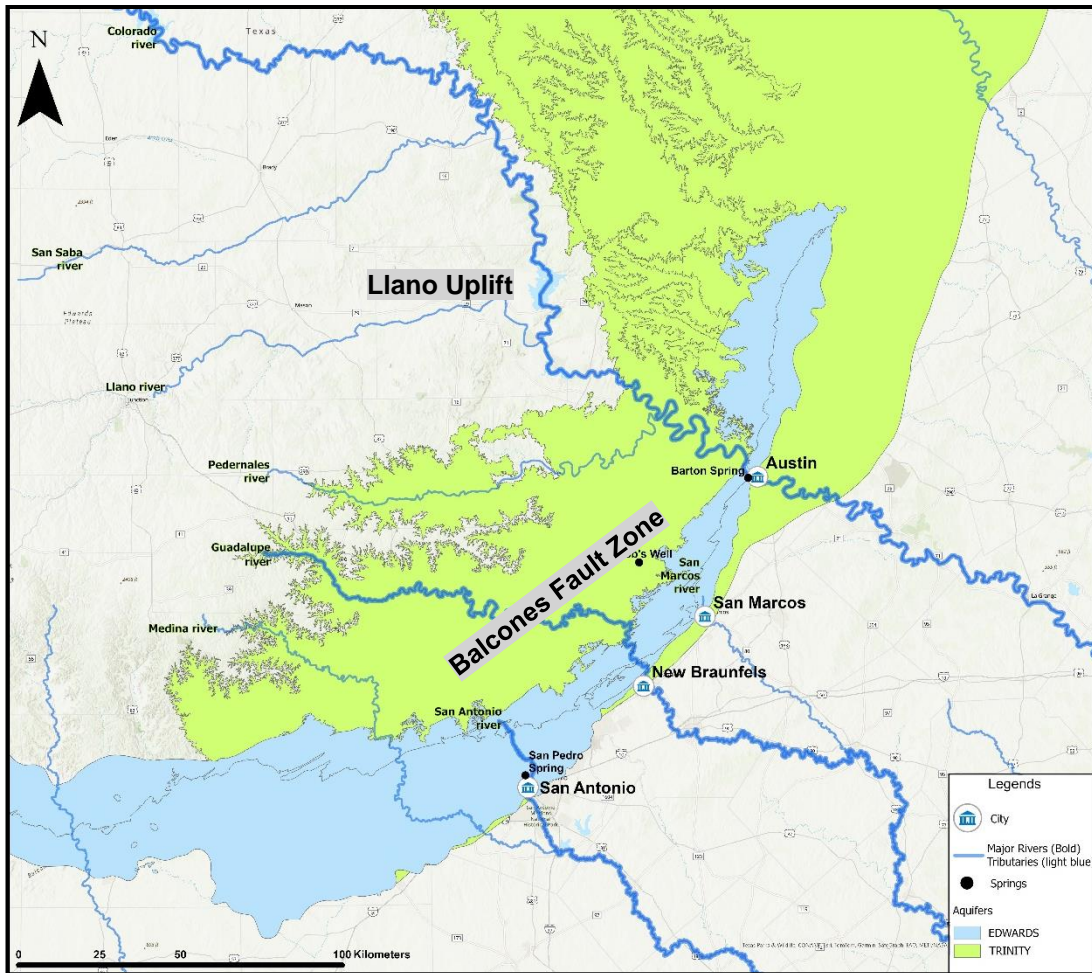


Figure 2: Edwards and Trinity aquifers map with Llano Uplift and BFZ region with rivers, springs, and city.

dissolution features, fault zones, and fractures (Ferrill et al., 2008). Over the course of geological time, the reactivation of the BFZ has resulted in displacement that has pushed the Edwards Aquifer laterally into contact with the Trinity Aquifer (Ferrill et al., 2008). The Texas Water

Development Board reports that the total subsurface area of the Edward Aquifer is about 2,480 square miles with a thickness of 200 to 600 feet, and the total subsurface area of the Trinity Aquifer is about 21,300 square miles with a thickness of 600 feet in North Texas and about 1,900 feet in central Texas (Fig. 2).

In addition, within the Llano Uplift region, lie three minor aquifers: the Ellenburger-San Saba, Hickory, and Marble Falls aquifers. These aquifers collectively cover a subsurface area of 12,811 square miles (Texas Water Development Board). The Ellenburger-San Saba aquifer being the largest of the three boasts a maximum thickness of 2,700 feet, while the Hickory aquifer reaches approximately 480 feet thick, and the Marble Falls aquifer has a maximum thickness of

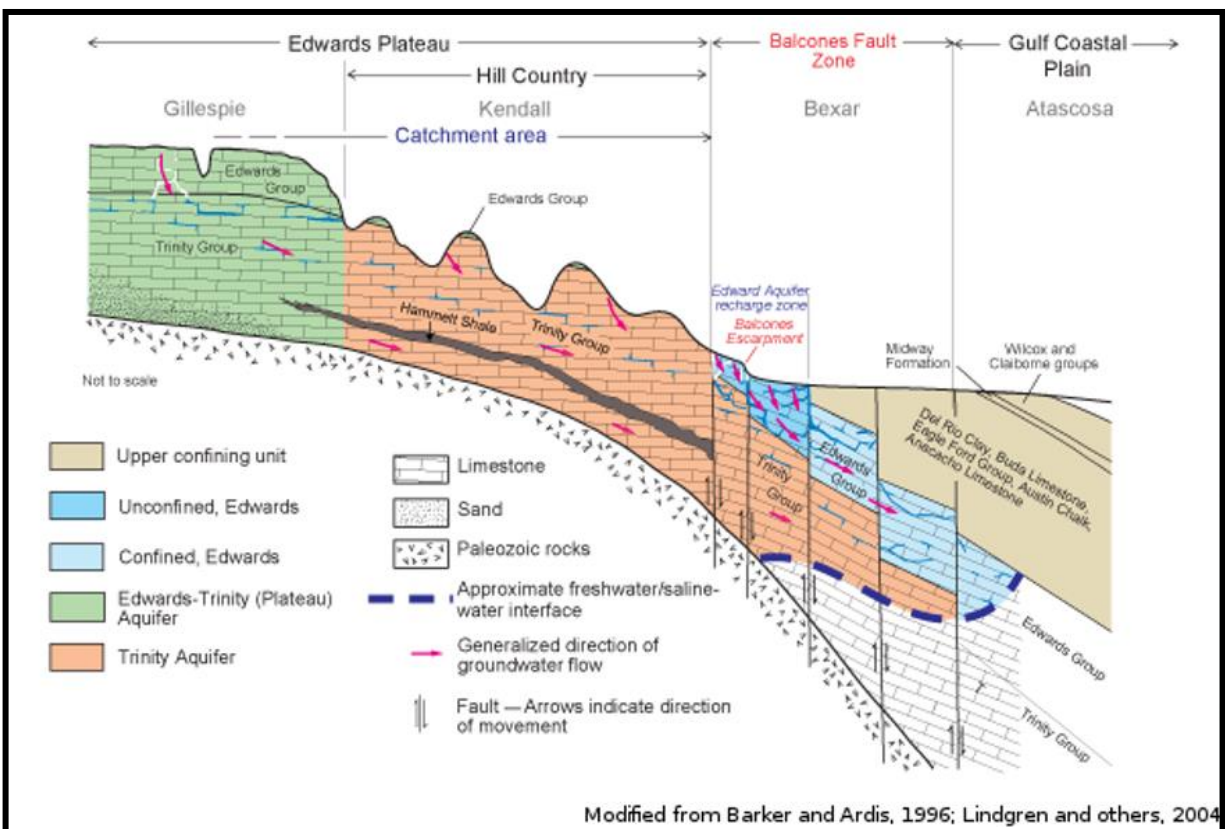


Figure 3: Modified cross-section figure by Texas State University modified from Barker and Ardis (1996) and Lindgren and others (2004). Trinity and Edwards aquifers cross section with different lithologies and structure.

600 feet. These minor aquifers are situated within a karst and faulted system within the Paleozoic Formations.

In surface environments, the study area encompasses networks of three major river systems and five tributaries, along with numerous springs (Fig. 2). The major rivers include the Colorado River, Guadalupe River, and San Antonio River. While the tributaries include the San Saba River, Llano River, Pedernales River, San Marcos River, and Medina River. Lastly, three large springs are the San Pedro Spring Pool, Barton Spring Pool, and Jacob's Well are all situated along the BFZ. These natural springs, in conjunction with the intricate river systems and aquifers, stand as vital components of the region's hydrological network, collectively bolstering its water resources for Texas.

CHAPTER 3: STRONTIUM AND URANIUM ISOTOPE GEOCHEMISTRY

3.1. Strontium Isotopes

Strontium is a relatively abundant trace metal and is classified within the divalent alkali-earth group. Strontium has three stable isotopes (^{84}Sr , ^{86}Sr , ^{88}Sr), and one radiogenic isotope (^{87}Sr). Moreover, strontium exhibits a high degree of solubility in a diverse range of aqueous solutions. The presence of ^{87}Sr in nature is primarily attributable to the beta decay process of ^{87}Rb , characterized by its extraordinarily extensive half-life of 4.88×10^{10} years. In natural water sources, strontium's occurrence is largely controlled by geological processes, with a prominent influence from the composition of the watershed lithology. $^{87}\text{Sr}/^{86}\text{Sr}$ ratios are reflected by the type and age of the lithological formation and provide insights into deeply-derived fluids, especially with older and different types of lithologies from surface environments (Mukhopadhyay & Brookins, 1976; Burke et al., 1982; Kirkland et al., 1995; McArthur et al., 2001; Van der Hoven & Quade, 2002; Young & Chan, 2017). Older lithologies, typically located

at greater depths, exhibit higher isotope ratios in comparison to younger lithologies found closer to the surface (Taggart & Brookins, 1975; Goff et al., 1994; Crossey et al., 2006).

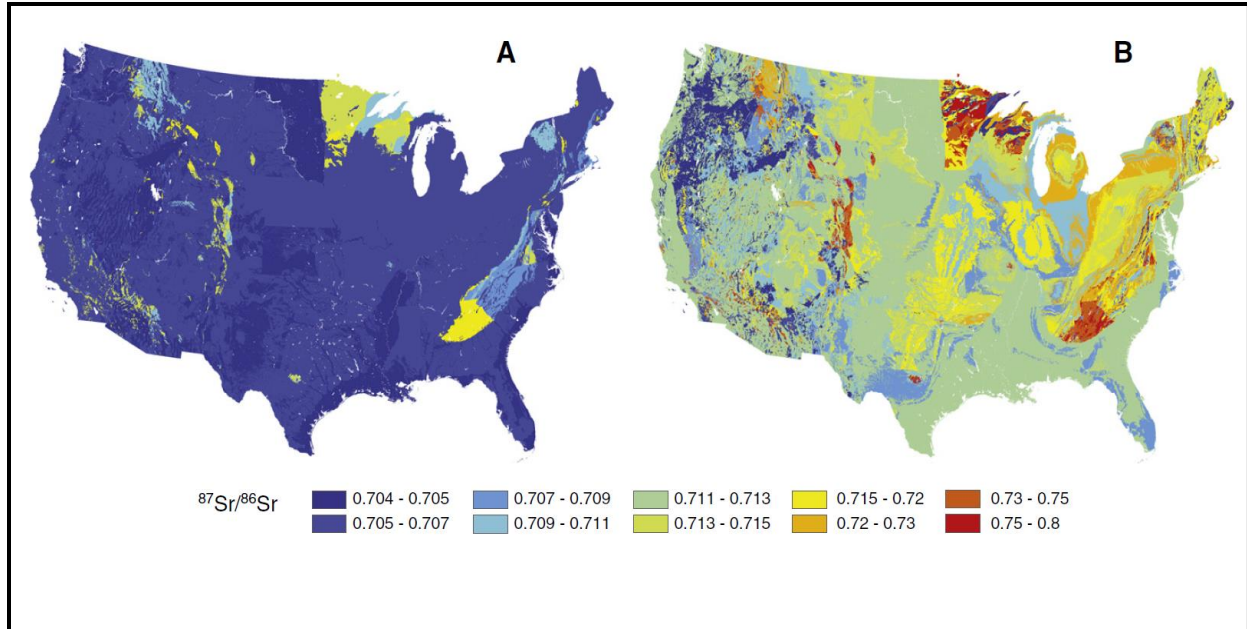


Figure 4: Modified diagram from Bataille & Bowen (2012) displaying Sr isotope ratios for major bedrock lithologies in the United States; (A) $^{87}\text{Sr}/^{86}\text{Sr}$ variations from bedrock models; (B) $^{87}\text{Sr}/^{86}\text{Sr}$ variations from bedrock age-only model.

Moreover, $^{87}\text{Sr}/^{86}\text{Sr}$ ratios can serve as a valuable tool for distinguishing between various lithologies, primarily because of the prolonged evolution of strontium ratios over time, a consequence of Rb/Sr fractionation (Table 1) (Bullen et al., 1996). For instance, when examining $^{87}\text{Sr}/^{86}\text{Sr}$ ratios in Precambrian granitic rocks or gneiss, we often observe higher values (≥ 0.710) due to the elevated Rb/Sr ratios within these old age rocks (Capo et al., 1998). This stands in contrast to sedimentary rocks, where isotopic composition tends to be influenced by ancient seawater ratios (~ 0.710). Furthermore, strontium is naturally released into fluid systems during the weathering of geological materials, and this process is characterized by minimal fractionation through weathering (Paces and Wurster, 2014). Due to these characteristics, the behavior of

$^{87}\text{Sr}/^{86}\text{Sr}$ ratio in a fluid is valuable in hydrogeochemical studies, shedding light on water-rock interactions in the study area and making them valuable lithologic fingerprints in river systems.

3.2. Uranium Isotopes

Uranium is a relatively scarce trace metal that occurs naturally in low concentration in water, soil, and rocks, with the majority originating from granitic deposits. Uranium is comprised of three isotopes (^{238}U , ^{235}U , and ^{234}U), each with its distinct level of radioactivity. ^{238}U and ^{235}U are notable for their exceptionally extended half-lives of 4.468×10^9 years and 7.038×10^8 years, respectively. In contrast, ^{234}U is relatively short-lived daughter isotope within the ^{238}U decay chain, with a half-life of about 2.4525×10^5 years (Cheng et al., 2000). The solubility of natural uranium is closely tied to the prevailing redox conditions. In surface water and shallow groundwater, when uranium becomes oxidized, it readily transforms into more soluble uranyl ions (UO_2^{2+}), capable of forming complexes with various ligands, including uranyl carbonate (Clark et al., 1995; Murphy and Shock, 1999).

In lithologies older than 1.25 million years, ^{234}U reaches a condition known as radioactive secular equilibrium with respect to ^{238}U which signifies that the rate of ^{234}U decay is equal to the rate of its production, resulting in a $^{234}\text{U}/^{238}\text{U}$ activity ratio of 1.0. However, elevated ^{234}U ratios in water derive from the displacement of $^{234}\text{U}/^{238}\text{U}$ atoms from the crystal lattice following the decay of ^{238}U and the subsequent recoil of the resulting ^{234}Th nuclide, following two successive decays, from ^{238}U to ^{234}Th , then to ^{234}Pa , and finally to the ^{234}U nuclide (Grabowski & Bem, 2011). Natural water typically exhibits a $^{234}\text{U}/^{238}\text{U}$ ratio greater than 1.0 (Chabaux et al., 2003). Indeed, as water interacts with these lithologies, it tends to selectively dissolve ^{234}U over ^{238}U due to the alpha-decay process (Porcelli and Swarzenski, 2003; Chabaux et al., 2008). This results in initial $^{234}\text{U}/^{238}\text{U}$ ratios greater than 1 in natural water. Following the

water-rock interactions, the $^{234}\text{U}/^{238}\text{U}$ ratio in water undergoes substantial alterations as a result of the alpha recoil process from surrounding aquifer matrix, where ^{238}U decays to ^{234}U and emits a high-energy alpha particle (Fleischer, 1980). Hence, uranium isotopes can serve as a natural tracer to distinguish the flow path of a fluid and determine the amount of time groundwater spends in the subsurface, as deeply sourced fluids generally exhibit higher $^{234}\text{U}/^{238}\text{U}$ ratios compared to fluids at the surface (Table 1) (Kronfeld, 1974; Chabaux et al., 2003; Chabaux et al., 2008). This unique groundwater signature primarily develops when water passes through a redox front within the aquifer, leading to a significant decrease in uranium solubility under reducing conditions (Langmuir, 1978; Drever, 1997). Consequently, the reduced uranium concentrations in groundwater, coupled with enhanced alpha recoil effects from the uranium-enriched aquifer matrix, can result in abnormally high $^{234}\text{U}/^{238}\text{U}$ ratios reaching up to 10 in deep carbonate aquifers in Texas while surface fluids are generally less than 3 (Kronfeld, 1974; Chabaux et al., 2003). The unique behavior of uranium in water-rock interactions is influenced by geological factors and the alpha recoil processes, making it a successful tracer in hydrogeochemical investigations for the study area.

Water Type	$^{234}\text{U}/^{238}\text{U}$	$^{87}\text{Sr}/^{86}\text{Sr}$
Surface water with short water-rock interactions times	1.1 - 1.42	-
Groundwater with long water-rock interactions times	0.92 - 12.25	-
*Kronfeld (1974)		
Lithology		
Precambrian Crystalline	-	0.711 - 0.72
Paleozoic Carbonates	-	0.708 - 0.711
Paleozoic Clastic	-	0.708 - 0.713
Mesozoic Carbonates	-	0.707 - 0.709
Mesozoic Clastic	-	0.707 - 0.709
Cenozoic Clastic	-	0.705 - 0.708
Cenozoic Sediments	-	0.705 - 0.708
*Bataille and Bowen (2012)		

CHAPTER 4: METHODS

4.1. Sample Collection

A total of twenty-nine water samples were collected in the study area in December 2022 (Fig. 5). Among them, twenty-six samples were sourced from surface water in river systems that flow southeastward across geological features of the Llano Uplift and the BFZ. These river samples were gathered at various strategic locations such as the Llano Uplift Region (LU - orange circle), the Balcones fault zone Region (BFZ - blue square), the In-between Llano Uplift

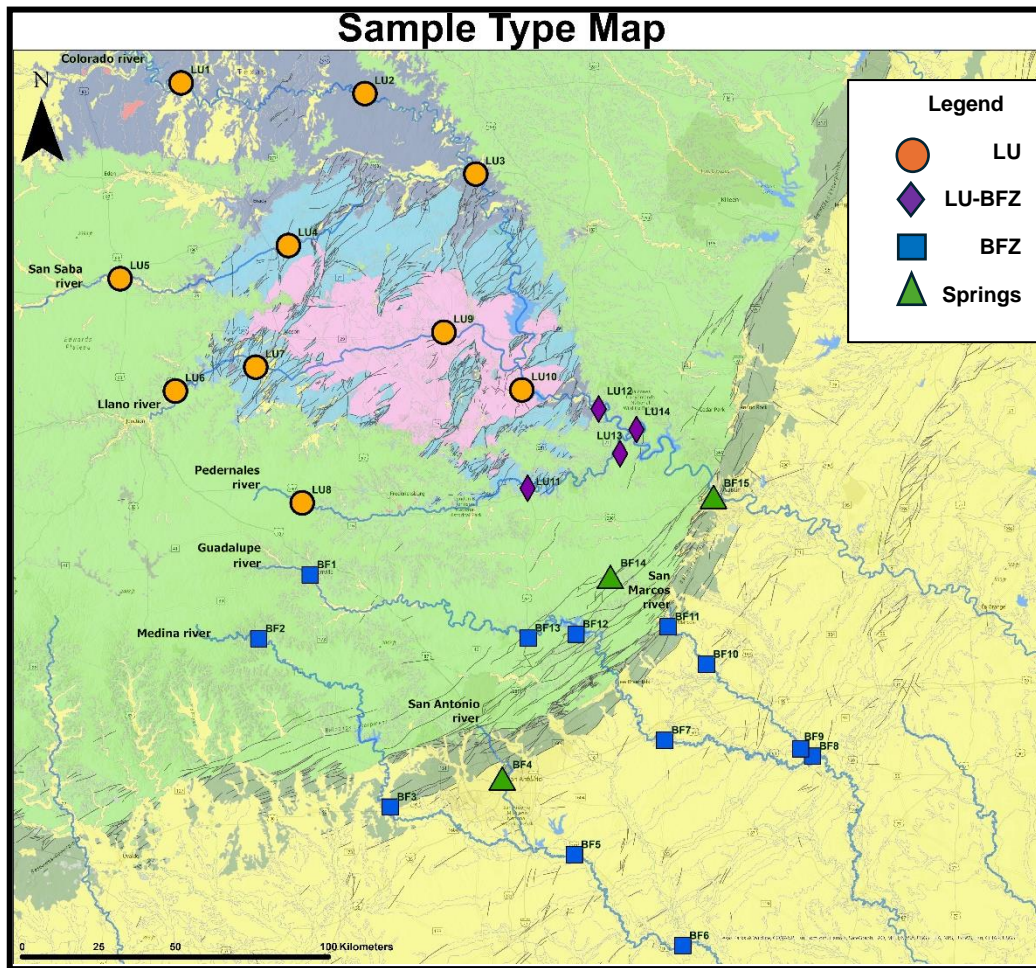


Figure 5: Sample map of the study area. Geology is the same as Fig.1A. LU - Llano Uplift; LU-BFZ – Llano Uplift to Balcones fault zone; BFZ – Balcones fault zone.

& Balcones fault zone (LU-BFZ – purple diamond), and springs (Springs – green triangle). The purpose of sample collection was twofold: First, samples were collected from upstream of, within, and downstream of the Llano uplift and BFZ to assess the influence of these geologic structures on river water chemistry: Second, samples were collected from a variety of lithologies to test for possible lithologic controls on river water chemistry.

A total of 10 samples were collected from the LU region. LU samples include samples from rivers located northwest of the Llano Uplift along the Colorado River, along with its tributaries such as the San Saba River, Llano River, and Pedernales River. The tributaries flow east through the Llano Uplift and eventually merge with the Colorado River, which then flows southeast towards the BFZ. The LU samples are grouped together primarily because the majority of its associated rivers and streams flow through or are in close proximity to the Llano Uplift.

Twelve samples were collected from adjacent to and within the BFZ. These samples are from rivers located in the southern part of the study area, including major rivers such as the Guadalupe River, San Marcos River, San Antonio River, and the Medina River. These rivers flow southeast across the BFZ and merge with one another. For example, the Medina River is a tributary to the San Antonio River, which is a tributary of the Guadalupe River. The BFZ samples are grouped together primarily because of its associated rivers and streams flowing southeast through the Balcones fault zone.

A total of four samples were collected from in between the Llano Uplift and the BFZ. These are referred to as LU-BFZ in Figure 5. These samples are from a relatively restricted region along the Colorado and Pedernales rivers, and it is located at close proximity to both large geologic structures.

The final three samples were collected from spring pools located along the BFZ, an essential recharge contributor to the river systems. These samples were collected to compare river water chemistry to the chemistry of the underlying aquifer systems.

Together, this strategic sampling approach was designed to explore whether geological structure and lithology exerts influence on the river water chemistry, and probe for the presence of deeply-derived fluids within the fault systems of the BFZ, providing critical insight into the hydrogeological dynamics of the region.

4.2. Sample Preparation for Geochemical Analysis: major elements, ($^{87}\text{Sr}/^{86}\text{Sr}$) and ($^{234}\text{U}/^{238}\text{U}$) ratios

The water samples were analyzed at the ICP (Inductively Coupled Plasma) Analytical Facility in the Department of Earth, Environmental and Resources Science at UTEP using Horiba ICP OES, Thermo iCap ICP MS, and Nu Plasma HR Multi-Collector ICP-MS and established analytical techniques for analyzing major and trace element concentrations, $^{87}\text{Sr}/^{86}\text{Sr}$ and $^{234}\text{U}/^{238}\text{U}$ ratios (Ma et al., 2010; Konter and Storm, 2014).

The water samples were filtered using an electric pump and a 0.45 μm membrane filter which effectively separates suspended particles and large colloids from the water samples. Subsequently, the filtered water was transferred into a 250 mL HDPE Nalgene bottle and three drops of concentrated HNO_3 were added to acidify samples for major and trace elements, $^{87}\text{Sr}/^{86}\text{Sr}$ and $^{234}\text{U}/^{238}\text{U}$ ratio analysis.

4.2.1. Major and trace elements

For the analysis of major and trace cation concentrations, approximately 15 mL of acidified sample were analyzed using a Horiba Optical Emission Spectrometer (OES) and

Thermo iCap ICP MS. During each run, the standards USGS M-210 and NIST 1640a were scrutinized between 3 to 5 times to evaluate measurement precision. The percent error of these standards did not exceed 10% for all major elemental concentrations. Concerning major anion concentrations, the non-acidified filtered sample underwent a tenfold dilution with deionized (DI) water (i.e., 10 mL of DI water for every 1 mL of sample). The precise dilution factor for each sample was determined using sample weights. These samples were then analyzed utilizing a Dionex ICS-2100. To ensure accuracy, an in-house water standard was assessed at least twice during each run. Overall, standard errors did not surpass 12%. Alkalinity values of the water samples were measured with an alkalinity titrator.

4.2.2. $^{87}\text{Sr}/^{86}\text{Sr}$ Analysis

To separate Sr isotopes from the sample matrix, the techniques described in Konter and Storm (2014) were followed, utilizing the Eichrom Sr-resin. A batch of twenty-nine acidified water samples were placed into 10mL Teflon beakers and allowed to evaporate overnight at 100°C on a hot plate. Subsequently, twenty-nine 0.2 mL columns were prepared, initially washed with 6 N HNO₃, and rinsed with DI water. These columns were then filled with Eichrom Sr-resin (150 mesh), cleaned using ultrapure water, and conditioned with 3.5 N HNO₃. Next, the dried samples were dissolved in 0.5 mL of 3.5 N HNO₃ and loaded onto the columns. The matrix was eluted in a series of steps by introducing varying amounts of 3.5 N HNO₃. Sr was collected in clean 15-mL Teflon beakers by adding 0.05 N HNO₃ to the columns. The Sr samples were left on a hot plate to dry overnight at 100°C. The isotopic ratios of $^{87}\text{Sr}/^{86}\text{Sr}$ were subsequently analyzed using the Nu Plasma MC-ICP-MS located at UTEP.

4.2.3. $^{234}\text{U}/^{238}\text{U}$ Analysis

To separate and purify U isotopes, the procedures described by Chabaux and colleagues (1995) were followed, utilizing ion chromatography. A batch of twenty-nine acidified water samples were placed into 10mL Teflon beakers and allowed to evaporate overnight at 100°C on a hot plate. Subsequently, twenty-nine 2 mL columns containing AG1-X8 anion resin (200-400 mesh) were prepared. These columns were initially washed with 6 N HCl and 0.25 HNO₃, rinsed with ultrapure water, and conditioned with 7.5 N HNO₃. Next, the dried samples were dissolved in 1 mL of 7.5 N HNO₃ and loaded into the prepared columns. The samples were then eluted with 7.5 N HNO₃. The U isotopes were collected in clean 15 mL Teflon beakers in a series of steps using ultrapure water, 0.5 N HCl, and 6 N HCl. These samples were then left on a hot plate to evaporate overnight at 100°C and re-dissolved in 0.2 mL of 6 N HCl. The purification for U isotopes was followed using 0.6 mL columns containing AG1-X8 anion resin (200-400 mesh). These columns were initially washed and rinsed with the same method as the 2 mL columns, with an additional wash with 0.5 N HCl, followed by conditioning with 6 N HCl. The dissolved samples were then introduced and followed by a series of elutions using 6 N HCl and acetone + 6 N HCl. Uranium isotopes were collected with 0.5 N HCl and evaporated overnight. Finally, the isotopic ratios of $^{234}\text{U}/^{238}\text{U}$ were analyzed using the Nu Plasma MC-ICP-MS located at UTEP.

4.3. GIS and Geological Data Integration and Analysis

The integration of the Geographic Information System (GIS) data is essential for this research as it allows for an in-depth analysis regarding the precise spatial alignment of the sample's location to the local and regional geology. GIS data were downloaded from the USGS and the Texas Water Development Board. These data include lithology type, ages, faults, rivers

and their associated spatial location and distribution. The precise spatial correlation between the sample's location and the local and regional geology is essential as it encompasses aspects such as geological structure information, lithological composition and age, and the extensive river systems that traverse the study area. The geological and geochemistry information are integrated and analyzed in GIS. This integration involves creating a geologic map that displays various rock types and their distribution, along with faults location. Following, the geochemical are superimposed onto the map as data points with graduated colors, each indicating their respective values for a comparative analysis with respect to lithology and spatial location.

This comprehensive integration serves as the keystone that aligns the research with the broader geological context, providing invaluable insights into how these environmental factors influence the variations observed in the major elements, $^{87}\text{Sr}/^{86}\text{Sr}$ and $^{234}\text{U}/^{238}\text{U}$ ratios within the sampled waters.

CHAPTER 5: RESULTS

5.1. Schematic Cross-Section

To compare geochemical trends with underlying lithologic units and rock ages, a schematic cross-section of the study area was constructed that trends northwest to southeast across the study area (Fig. 6). The lithologies of the northwest region of the study area are predominantly Paleozoic silicates rocks, minor evaporites, and Cenozoic unconsolidated sediments. Moving southward, the lithologies shift to predominantly Mesozoic carbonates surrounding Proterozoic igneous and metamorphic rocks of the Llano Uplift. The expanse of carbonates continues until reaching east of the BFZ, where a transition occurs to Cenozoic sedimentary rocks and unconsolidated sediments.

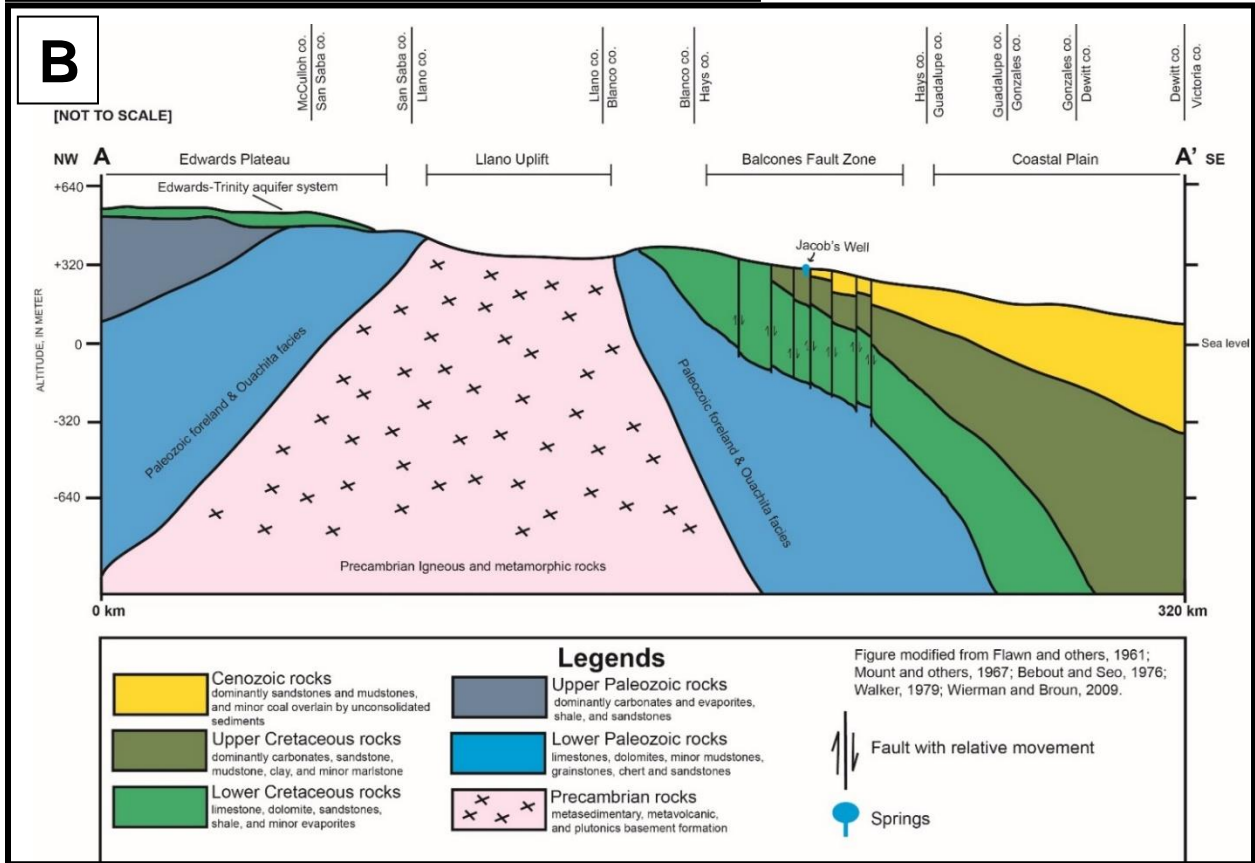
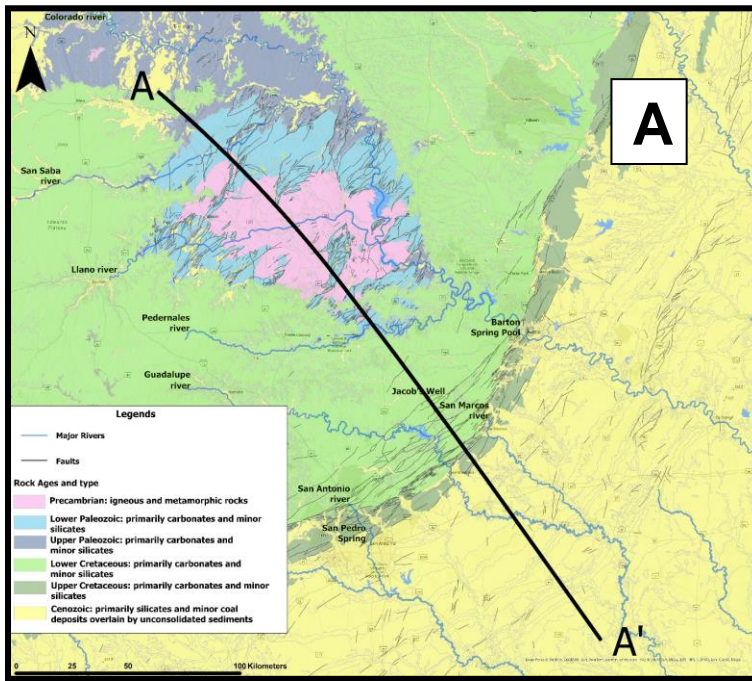


Figure 6: A-A' (A) Geologic map with rock units, rivers, and faults, showing the location of the cross-section. (B) Schematic cross-section of the study area highlighting major rock types and structures.

Table 2. River Samples and Springs data

Sample Name	Sample Type	River & Springs	Latitude	Longitude	Elevation (m)	Temp (C)	pH	Cond (µS/cm)
LU1	LU	Colorado	31.493525	-99.575143	497.4	17.2	7.78	550
LU2	LU	Colorado	31.458556	-98.942556	399	16.9	7.6	599
LU3	LU	Colorado	31.218639	-98.564611	337.4	15.8	7.83	449.8
LU4	LU	San Saba	31.014139	-99.209417	455.3	14.7	8.26	343.2
LU5	LU	San Saba	30.919139	-99.785861	566.6	15.6	8.02	389.5
LU6	LU	Llano	30.588694	-99.598000	466.3	17.7	8.2	331.7
LU7	LU	Llano	30.657694	-99.324139	413.9	16.2	8.25	297.8
LU8	LU	Pedernales	30.257750	-99.168972	559.9	16.8	8.46	330.1
LU9	LU	Llano	30.755194	-98.680222	297.2	17.2	8.28	311.4
LU10	LU	Colorado	30.582806	-98.417389	242.9	16.8	8.27	405.1
LU11	LU-BFZ	Pedernales	30.293611	-98.402083	325.8	16.9	8.36	474.6
LU12	LU-BFZ	Colorado	30.523111	-98.156278	202.7	16.6	8.25	420.6
LU13	LU-BFZ	Pedernales	30.390944	-98.085972	219.4	15	8.32	466.8
LU14	LU-BFZ	Colorado	30.460833	-98.028778	192	17.2	8.34	399
BF1	BFZ	Guadalupe	30.046528	-99.143556	487	14.6	8.24	333.2
BF2	BFZ	Medina	29.859889	-99.319417	478.2	13.3	8.15	326.8
BF3	BFZ	Medina	29.362111	-98.879806	228.3	15.7	7.83	468.8
BF4	Springs	San Pedro Spring	29.446889	-98.501778	198.7	18.6	7.72	860
BF5	BFZ	San Antonio	29.215194	-98.262750	105.5	19.2	8.54	1461
BF6	BFZ	San Antonio	28.942222	-97.904389	63.4	19.1	8.21	1211
BF7	BFZ	Guadalupe	29.546917	-97.951861	132.9	19.1	7.97	410.8
BF8	BFZ	Guadalupe	29.490972	-97.454611	65.2	19.8	7.9	420.4
BF9	BFZ	San Marcos	29.513667	-97.494472	122.8	17.4	7.9	377
BF10	BFZ	San Marcos	29.767500	-97.806222	136.5	18.2	7.95	501
BF11	BFZ	San Marcos	29.880028	-97.932917	152.4	20.2	7.85	540
BF12	BFZ	Guadalupe	29.862778	-98.245472	285.6	15.5	8.33	286.4
BF13	BFZ	Guadalupe	29.853333	-98.407361	296.3	13.5	8.11	389
BF14	Springs	Jacob's Well	30.034472	-98.126111	279.8	20.8	7.41	508
BF15	Springs	Barton Spring	30.263806	-97.770944	131.1	21.4	7.43	611

Table 3. Major Elements (ppm)

Sample Name	Sample Type	Ca	K	Mg	Na	S	Si	Cl	SO4	F	NO3	Br	PO4	HCO3
LU1	LU	54.42	6.81	21.80	52.86	26.62	1.78	107.45	90.52	0.17	2.53	0.92	0.07	125.46
LU2	LU	55.62	7.16	21.46	64.06	25.69	2.04	132.77	90.26	0.23	2.79	0.96	0.02	114.23
LU3	LU	67.43	4.59	24.89	24.21	6.28	5.36	59.43	24.61	0.12	3.36	nd	0.03	266.91
LU4	LU	52.71	2.24	25.16	13.07	3.53	4.52	41.55	17.55	0.20	1.30	nd	0.07	231.86
LU5	LU	69.92	1.88	24.90	12.45	3.22	5.90	41.03	17.37	0.24	2.54	nd	0.06	280.71
LU6	LU	56.37	1.60	21.26	8.80	2.43	6.34	30.23	15.51	0.22	0.96	nd		233.26
LU7	LU	43.45	1.61	21.90	8.81	2.53	5.63	37.87	14.11	0.19	0.68	nd	0.06	186.06
LU8	LU	40.21	2.07	27.68	30.84	8.38	6.66	63.83	34.72	0.18	1.32	0.49	0.07	193.26
LU9	LU	41.98	2.35	22.27	12.18	3.62	3.08	41.14	18.28	0.21	0.60	0.48	0.28	182.70
LU10	LU	40.92	6.08	25.58	35.31	7.23	3.63	79.48	29.06	0.24	1.01	0.74	0.08	183.51
LU11	LU-BFZ	43.75	4.70	37.13	36.90	11.72	5.52	80.52	46.13	0.26	1.00	0.87	0.09	229.42
LU12	LU-BFZ	42.58	5.99	26.11	36.97	7.70	3.67	78.63	30.67	0.23	1.04	0.62	0.13	194.90
LU13	LU-BFZ	47.66	3.80	39.72	35.13	14.61	5.98	75.20	52.53	0.28	1.14	0.62	0.02	249.29
LU14	LU-BFZ	40.95	5.20	25.57	30.06	7.38	4.75	69.71	28.56	0.22	1.16	0.87	0.08	185.52
BF01	BFZ	58.65	1.49	25.17	11.33	3.33	6.69	29.15	18.95	0.16	0.59	nd	0.02	264.46
BF02	BFZ	66.83	0.86	23.42	5.38	7.16	6.18	31.29	29.27	0.13	0.89	nd	0.01	246.63
BF03	BFZ	98.10	3.21	21.54	17.00	18.26	7.70	37.19	67.04	0.21	4.59	nd	0.06	305.17
BF04	Springs	60.77	1.90	11.35	149.12	41.74	8.90	169.23	145.61	0.36	2.19	nd		163.54
BF05	BFZ	87.56	25.22	33.97	240.94	45.70	4.19	353.38	158.94	0.73	49.12	6.59	2.73	260.69
BF06	BFZ	83.43	21.05	26.25	197.47	38.20	4.66	284.92	128.98	0.58	41.13	4.96	2.24	250.55
BF07	BFZ	71.51	3.51	16.28	17.45	10.35	5.69	48.98	36.66	0.23	9.17	nd	0.20	212.86
BF08	BFZ	68.46	4.68	15.45	23.23	9.92	3.89	46.81	32.18	0.17	4.23	nd	0.19	230.80
BF09	BFZ	56.81	6.15	9.69	33.61	11.94	5.53	61.51	44.51	0.20	4.17	nd	0.27	154.93
BF10	BFZ	98.55	2.56	21.00	19.15	11.00	6.25	53.99	39.22	0.18	7.10	nd	0.07	312.49
BF11	BFZ	109.70	1.54	20.35	12.37	9.84	6.10	44.60	36.23	0.16	6.12	nd	0.05	344.54
BF12	BFZ	40.59	2.28	20.37	12.64	6.61	5.59	46.30	27.02	0.25	0.85	0.49	0.09	149.72
BF13	BFZ	69.97	2.29	25.25	17.88	7.05	5.28	56.60	28.40	0.21	0.47	0.24	0.03	258.95
BF14	Springs	103.78	1.30	23.30	6.96	9.57	5.52	32.26	34.01	0.23	2.63	nd		354.22
BF15	Springs	98.40	1.80	26.35	24.51	12.73	6.19	62.82	44.97	0.27	6.34	nd	0.05	330.56

5.2. Electrical Conductivity

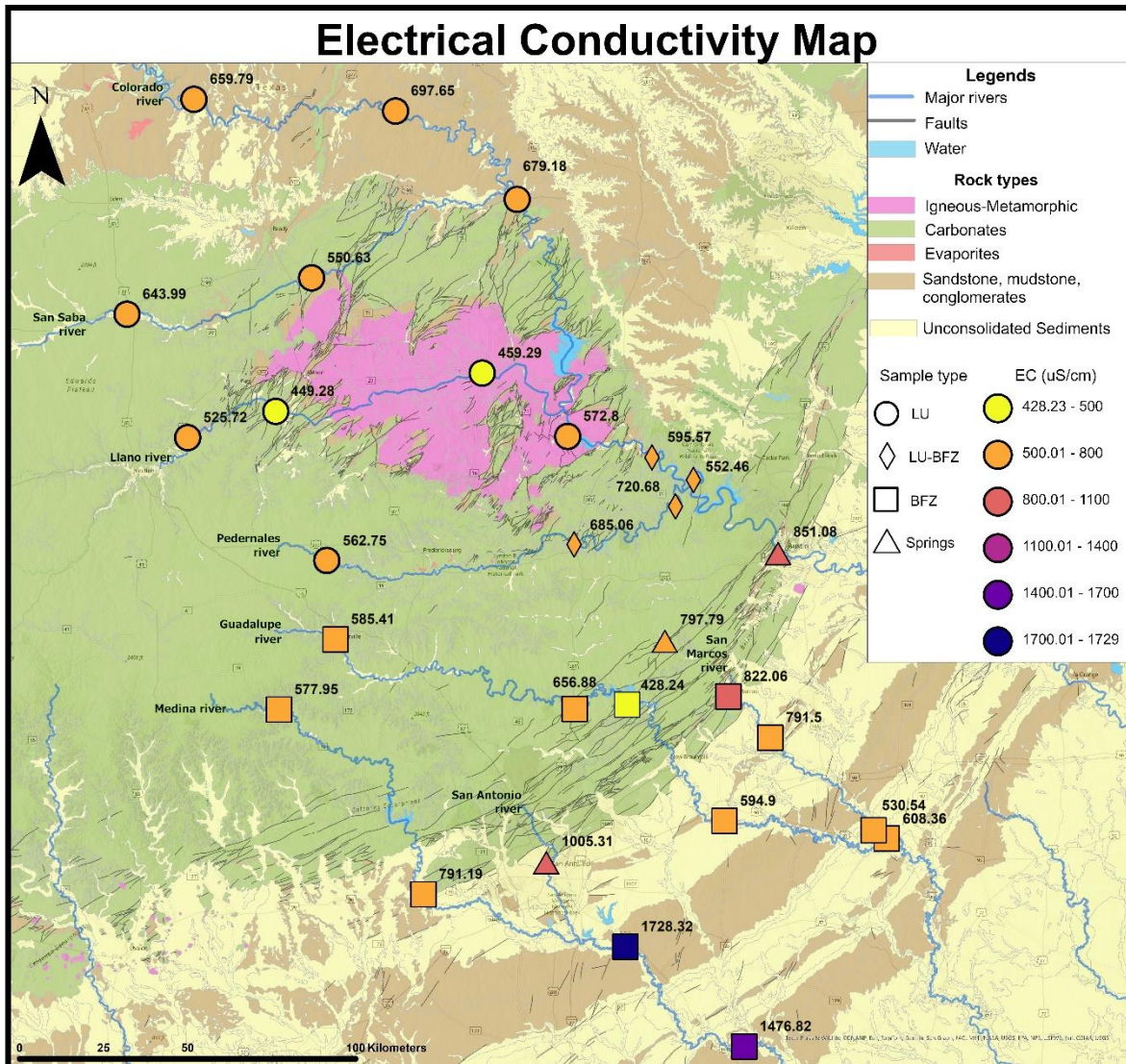


Figure 7: Electrical conductivity (EC) of samples collected in this study. Samples are grouped by location (different symbols) and color-coded by EC value.

Figure 7 and Table 2 show the measured electrical conductivity (EC) across the study area. Moving from the northwest to the south-southwest of the Llano Uplift, EC results are predominantly in the range of 500 to 800 $\mu\text{S}/\text{cm}$, represented by orange color, while values less than 500 $\mu\text{S}/\text{cm}$ are depicted as yellow color west of and within the Llano Uplift. Along the BFZ, EC values show an increase to 1005 $\mu\text{S}/\text{cm}$. The EC then decreases below 800 $\mu\text{S}/\text{cm}$ at San

Marcos and Guadalupe River southeast of the BFZ. Moving further southeast, the EC dramatically increases at the San Antonio River in two river samples, with values of 1476 and 1728 $\mu\text{S}/\text{cm}$.

5.3. Bicarbonate (HCO_3)

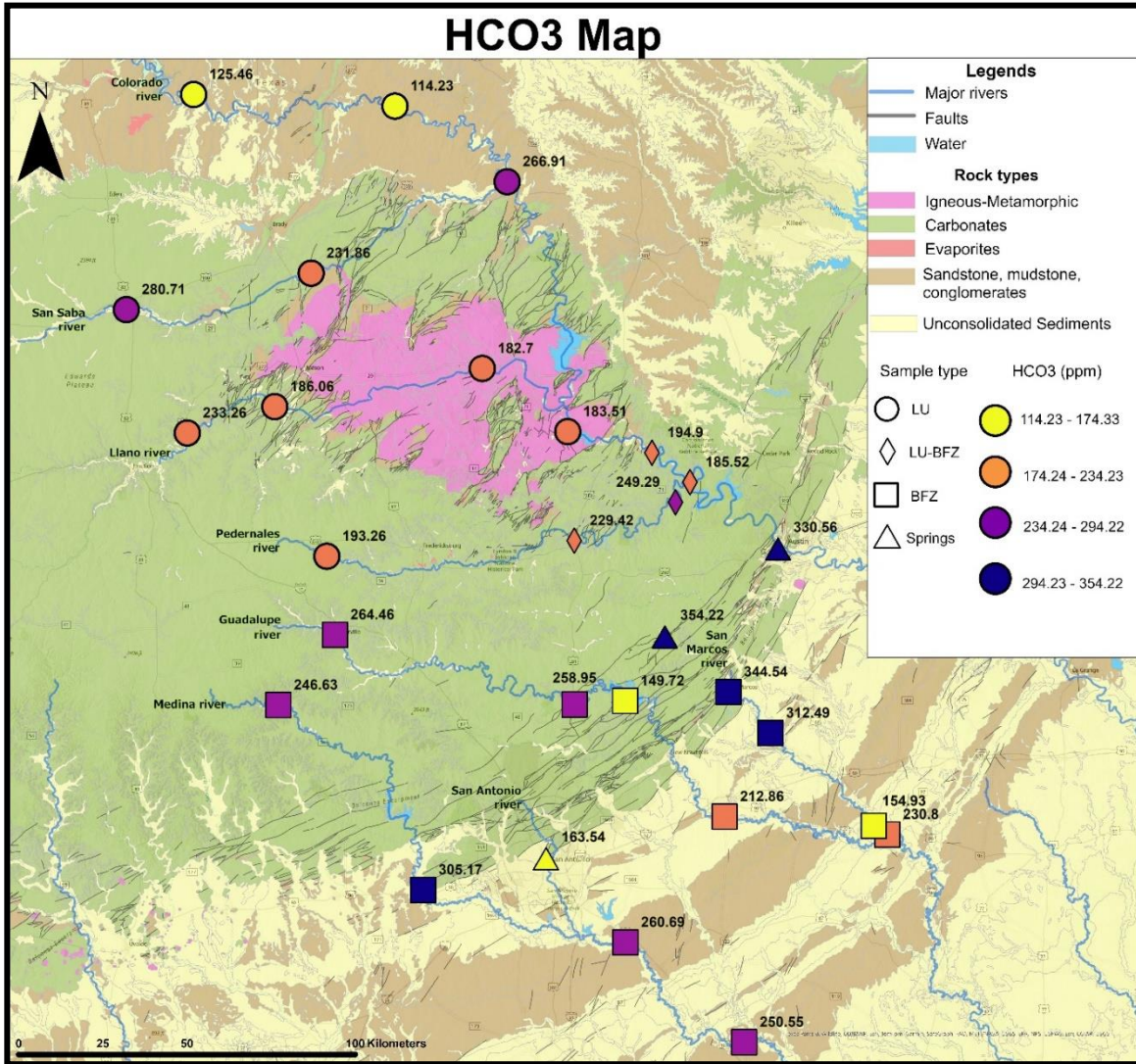


Figure 8: Bicarbonate (HCO_3) samples collected in this study. Samples are grouped by location (different symbols) and color-coded by HCO_3 value.

Figure 8 shows the measured bicarbonate (HCO_3) concentrations (ppm) across the study area. In the Llano Uplift region, the HCO_3 values are comparatively low compared to the rest of the dataset, ranging from 114.23 to 280.7 ppm. Similarly, the LU-BFZ samples also show a

relatively low HCO₃ values ranging from 185.5 to 249.2 ppm. Moving across the BFZ, samples show an increase in HCO₃ ranging from 149.7 to 344.5 ppm, with some of the highest values are along the fault zone. Finally, the spring samples show an intermediate range of 163.5 to 354.2 ppm.

Sample Name	⁸⁷ Sr/ ⁸⁶ Sr	+/- (2SE)	Sr (ppm)
LU1	0.7084	0.00001	0.777
LU2	0.70876	0.00004	0.625
LU3	0.70973	0.00002	0.209
LU4	0.70821	0.00002	0.466
LU5	0.70816	0.00002	0.562
LU6	0.708	0.00002	0.325
LU7	0.70796	0.00004	0.286
LU8	0.708	0.00002	0.317
LU9	0.70917	0.00002	0.226
LU10	0.71011	0.00002	0.308
LU11	0.70871	0.00003	0.28
LU12	0.71013	0.00002	0.312
LU13	0.70819	0.00001	0.475
LU14	0.70967	0.00003	0.318
BF1	0.70793	0.00002	0.249
BF2	0.70764	0.00002	0.308
BF3	0.70779	0.00001	0.655
BF4	0.70797	0.00002	0.482
BF5	0.70819	0.00002	0.794
BF6	0.70826	0.00004	0.683
BF7	0.70804	0.00002	0.467
BF8	0.70806	0.00002	0.501
BF9	0.7082	0.00003	0.394
BF10	0.70793	0.00002	0.517
BF11	0.70797	0.00003	0.513
BF12	0.70786	0.00004	0.326
BF13	0.7079	0.00003	0.564
BF14	0.70783	0.00002	0.6
BF15	0.70798	0.00002	2.669

5.4. $^{87}\text{Sr}/^{86}\text{Sr}$ Results

A total of 29 samples were analyzed for $^{87}\text{Sr}/^{86}\text{Sr}$ ratio (Table 4). Overall ratios range from 0.7076 to 0.7103. In the Llano Uplift region, sample ratios are relatively high compared to the rest of the entire dataset, ranging from 0.7079 to 0.7101 (Fig. 9). The highest ratios are within and adjacent to the Llano Uplift. The LU-BFZ samples also show very high $^{87}\text{Sr}/^{86}\text{Sr}$ ratios, ranging from 0.7081 to 0.7101. The BFZ samples show a sudden decrease in $^{87}\text{Sr}/^{86}\text{Sr}$ ratios,

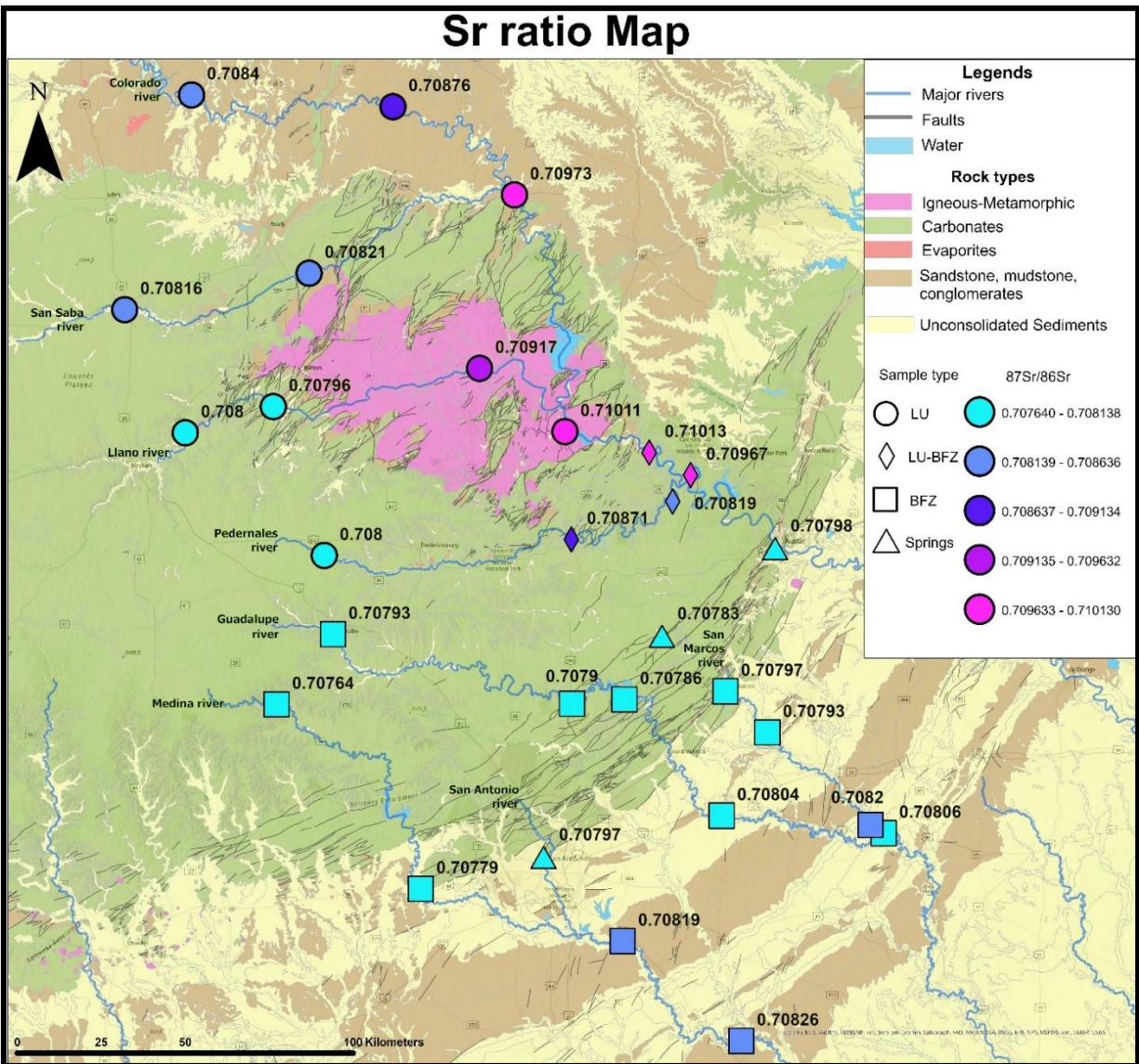


Figure 9: $^{87}\text{Sr}/^{86}\text{Sr}$ ratios of samples collected in this study. Samples are grouped by location (different symbols) and color-coded by Sr ratio.

ranging from 0.7076 to 0.7082. Finally, the three springs sample show ratios that are intermediate, ranging from 0.7078 to 0.7079.

The $^{87}\text{Sr}/^{86}\text{Sr}$ ratio can also be organized by river to investigate possible changes within a single river system as it flows downstream. A total of six samples are from the Colorado River. $^{87}\text{Sr}/^{86}\text{Sr}$ ratios are relatively low within the upstream region of the Colorado River, increase within the Llano Uplift, and decrease again by the time the Colorado River crosses the BFZ (Fig. 9). The four highest $^{87}\text{Sr}/^{86}\text{Sr}$ ratios of the entire dataset are from the central reaches of the Colorado River. Tributaries of the Colorado River have smaller sample size, but some of them share similar trends. The San Saba, Llano, and Pedernales rivers flow east and intersect the Llano Uplift. All three rivers show a slight increase in $^{87}\text{Sr}/^{86}\text{Sr}$ across the Llano Uplift before merging with the Colorado River. In contrast, the Guadalupe, San Marcos, and San Antonio, and Medina rivers flow southeast across the study area without merging with the Colorado River. A total of 14 samples were collected from these four rivers. $^{87}\text{Sr}/^{86}\text{Sr}$ ratios are relatively low and consistent along the length of each river through the BFZ, before showing a slight increase within the Cenozoic sediments downstream of the BFZ (Fig. 9).

Sample Name	$^{234}\text{U}/^{238}\text{U}$	+/- (2SE)	^{238}U (ppb)
LU1	1.53	0.004	0.79
LU2	1.461	0.004	0.77
LU3	2.05	0.004	0.28
LU4	1.456	0.004	0.35
LU5	1.392	0.003	0.33
LU6	1.22	0.004	0.26
LU7	1.331	0.004	0.64
LU8	1.145	0.003	1.02
LU9	1.871	0.005	0.83
LU10	1.685	0.005	0.72
LU11	1.813	0.005	0.99
LU12	1.703	0.006	0.79
LU13	1.623	0.004	0.61
LU14	1.673	0.005	0.86
BF1	1.158	0.003	0.57
BF2	1.143	0.013	0.2
BF3	1.21	0.004	0.29
BF4	1.186	0.005	0.38
BF5	1.188	0.003	0.66
BF6	1.211	0.003	0.6
BF7	1.187	0.003	0.54
BF8	1.193	0.002	0.59
BF9	1.234	0.004	0.5
BF10	1.172	0.003	0.53
BF11	1.166	0.004	0.25
BF12	1.114	0.006	0.67
BF13	1.147	0.014	0.65
BF14	1.222	0.003	0.48
BF15	1.191	0.004	0.39

5.5. $^{234}\text{U}/^{238}\text{U}$ Results

A total of 29 samples were analyzed for $^{234}\text{U}/^{238}\text{U}$ ratios (Table 5). Overall ratios range from 1.1 to 2.05. In the Llano Uplift region, samples are relatively high compared to the rest of the dataset, ranging from 1.1 to 2.05 (Fig. 10). The highest ratios are within and adjacent to the

Llano Uplift. The LU-BFZ samples also show very high $^{234}\text{U}/^{238}\text{U}$ ratios ranging from 1.6 to 1.8. The BFZ shows a sudden decrease in $^{234}\text{U}/^{238}\text{U}$ ratio, ranging from 1.1 to 1.2. Finally, the three springs sample show ratios that are intermediate, ranging from 1.1 to 1.2.

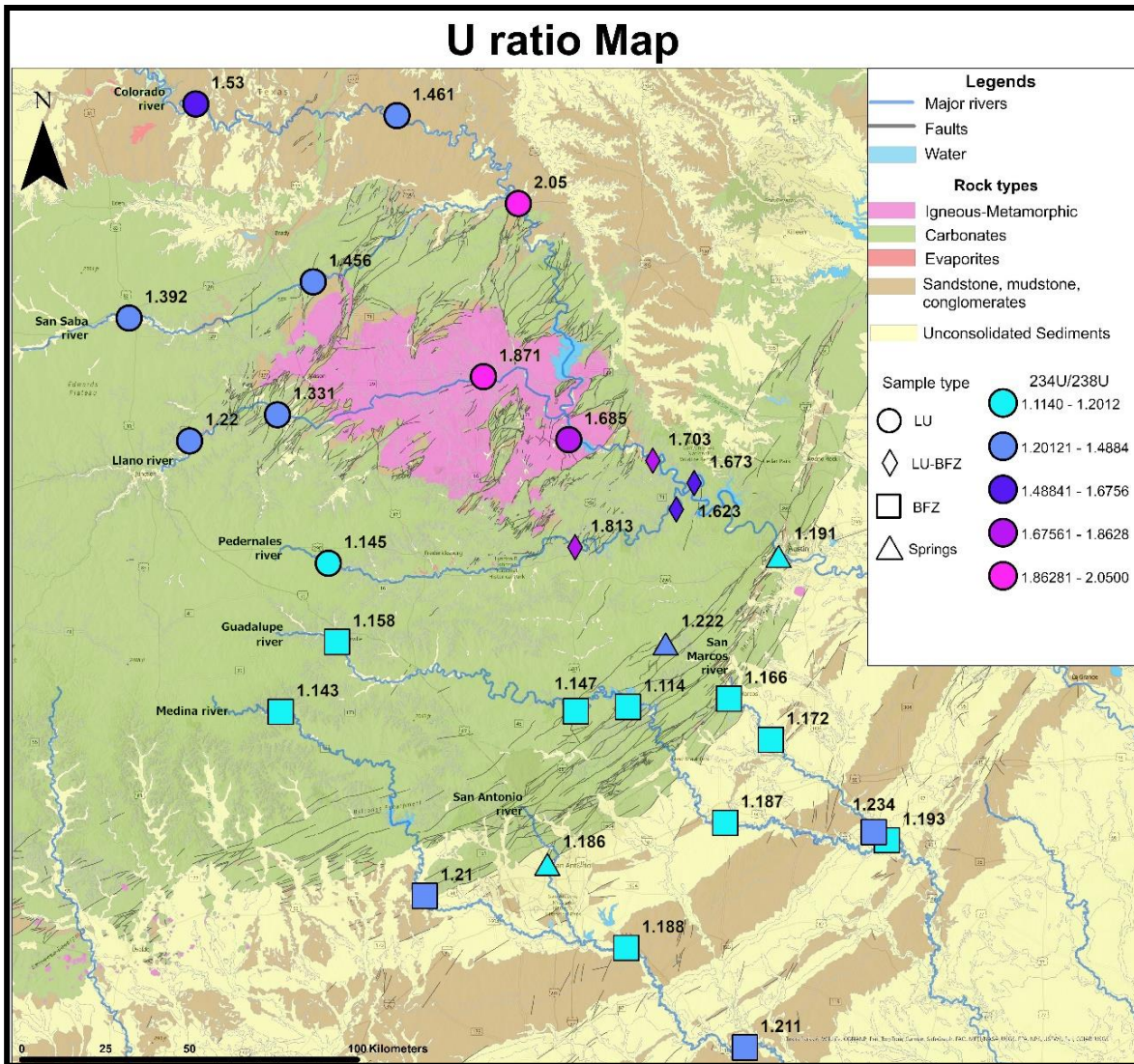


Figure 10: $^{234}\text{U}/^{238}\text{U}$ ratios of samples collected in this study. Samples are grouped by location (different symbols) and color-coded by U ratio.

The $^{234}\text{U}/^{238}\text{U}$ ratio can also be organized by river to investigate possible changes within a single river system as it flows downstream. A total of six samples are from the Colorado River. $^{234}\text{U}/^{238}\text{U}$ ratios are relatively low within the upstream region of the Colorado River, increase within the Llano Uplift, and decrease by the time the Colorado River crosses the BFZ (Fig. 10).

The highest $^{234}\text{U}/^{238}\text{U}$ ratios of the entire dataset are from the central reaches of the Colorado River. Tributaries of the Colorado River have a smaller sample size, but some of them share similar trends. The San Saba, Llano, and Pedernales rivers flow east and intersect the Llano Uplift with the second highest $^{234}\text{U}/^{238}\text{U}$ ratio from the Llano River. All three rivers show an increase in $^{234}\text{U}/^{238}\text{U}$ ratio across the Llano Uplift before merging with the Colorado River. In contrast, The Guadalupe, San Marcos, and San Antonio, and Medina rivers flow southeast across the study area without merging with the Colorado River. A total of 14 samples were collected from these four rivers. $^{234}\text{U}/^{238}\text{U}$ ratios are relatively low and consistent along the length of each river through the BFZ, before showing a slight increase within the Cenozoic sediments downstream of the BFZ (Fig. 10).

5.6. Geochemical Trends

In this section I present various scatter plots to highlight relationships between EC, HCO_3 , major elements, Sr, and U datasets of these river water samples. To do that, I use the four groups of data that were defined previously. These include LU samples, BFZ samples, LU-BFZ samples, and spring samples, each shown as a distinct color and shape that corresponds to Figure 4.

5.6.1. Trends in Electrical Conductivity (EC)

EC is plotted against Sr concentrations in Figure 11A. Most samples plot at low Sr and EC values, including all samples from the LU and spring groups. However, LU samples might also show a slight positive trend that is difficult to identify because of the restricted range in Sr and EC. The BFZ samples display the greatest range in EC (Fig. 11). These samples overlap with

LU and spring samples, but also contain elevated EC. All three of the spring samples show slightly elevated EC values compared to most other samples.

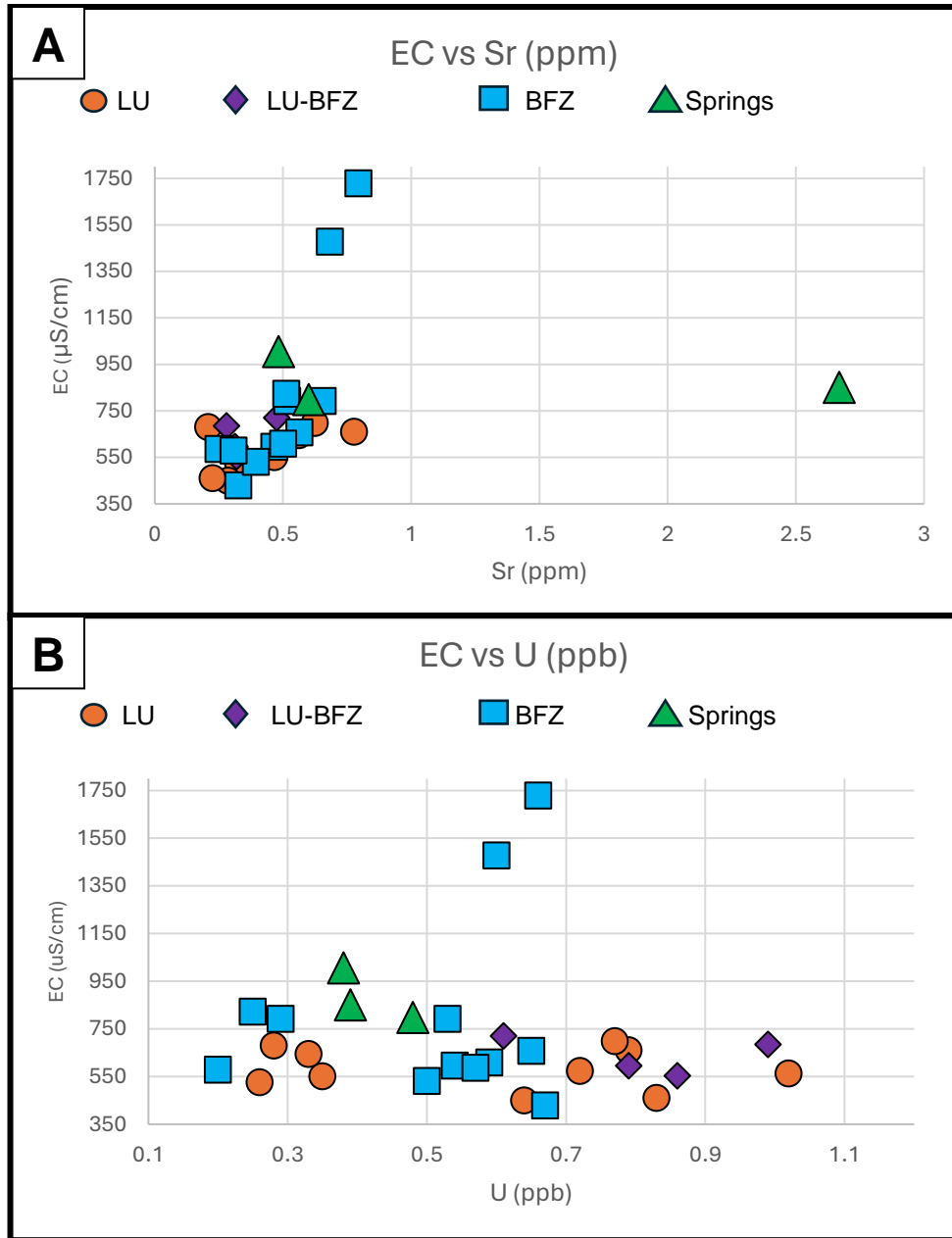


Figure 11: (A) EC (us/cm) vs Sr (ppm) and (B) U (ppb) plots with different sample types. Llano Uplift (orange circle), in-between LU and BFZ (purple diamond), Balcones fault zone (blue square), and springs (green triangle).

Whereas EC shows a slight positive correlation with Sr (Fig. 11A), on a plot of U vs. EC, the entire dataset displays a slight negative trend (Fig. 11B). All sample groups have a range of

U values between 0 and 1 ppb. Spring samples are the most clustered at intermediate U and slightly elevated EC values. LU samples have a wider range of U (0.26 ppb to 0.83 ppb) than other sample groups. LU-BFZ samples have the highest U values. BFZ also show a range in U, but at low to intermediate values.

5.6.2. Trends in Bicarbonate (HCO_3)

All sample groups show a wide range in bicarbonate (Figs. 12). LU samples show low to intermediate HCO_3 (114 ppm to 280 ppm), whereas BFZ samples are low to high (150 ppm to 340 ppm). LU-BFZ displays more restricted intermediate HCO_3 values ranging from 185 ppm to 250 ppm. Two of the spring samples show high HCO_3 and one spring sample is low. Since Sr ppm is low for all but 1 sample, the entire dataset plots along a horizontal array on a plot of HCO_3 vs. Sr (Fig. 12A). When HCO_3 is plotted against U (Fig. 12B), the dataset shows a negative trend, where high U values correspond to low HCO_3 , and high HCO_3 corresponds to the lowest U values. This trend is also evident in The LU and BFZ sample groups. LU-BFZ samples might also show a similar trend but have restricted HCO_3 values. The spring samples, however, form a nearly horizontal trend at U values of ~ 0.4 ppb across a wide range of HCO_3 .

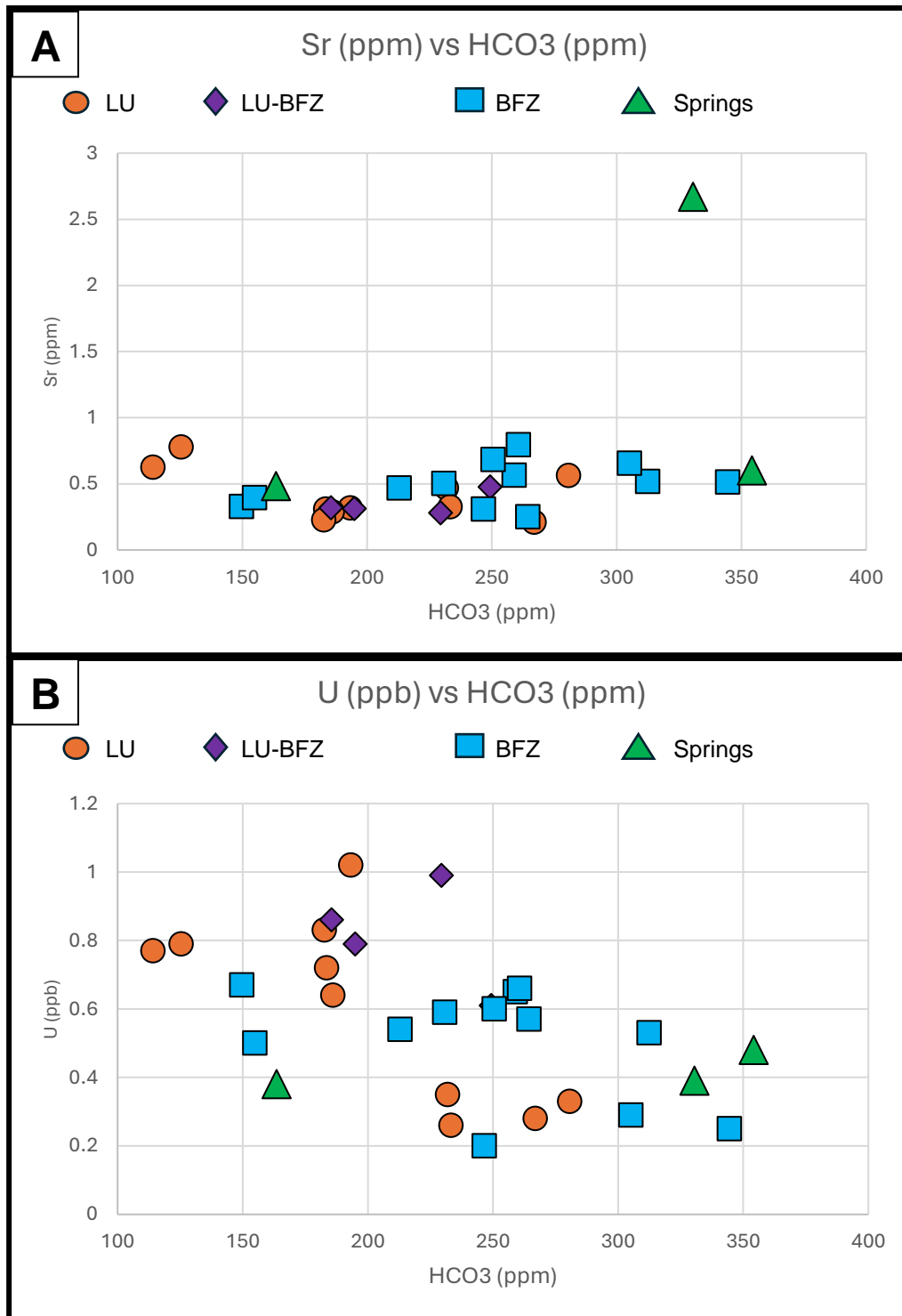


Figure 12: (A) Sr and (B) U vs HCO₃ plots with different sample types. Llano Uplift (orange circle), in-between LU and BFZ (purple diamond), Balcones fault zone (blue square), and springs (green triangle).

5.6.3. Trends in Major Elements

Ratios of major elements offer additional insight into possible water sources and possible influence of lithology. Figure 13 displays Mg/Na plotted against Ca/Na from Table 3. Together, the data form a positive array. LU, BFZ, and spring samples have a wide range in Mg/Na and Ca/Na. The LU sample array has a slightly lower slope than the BFZ sample array. LU-BFZ samples are anomalous compared to the other three groups. They have low Ca/Na ratios and low to intermediate Mg/Na that form a horizontal array.

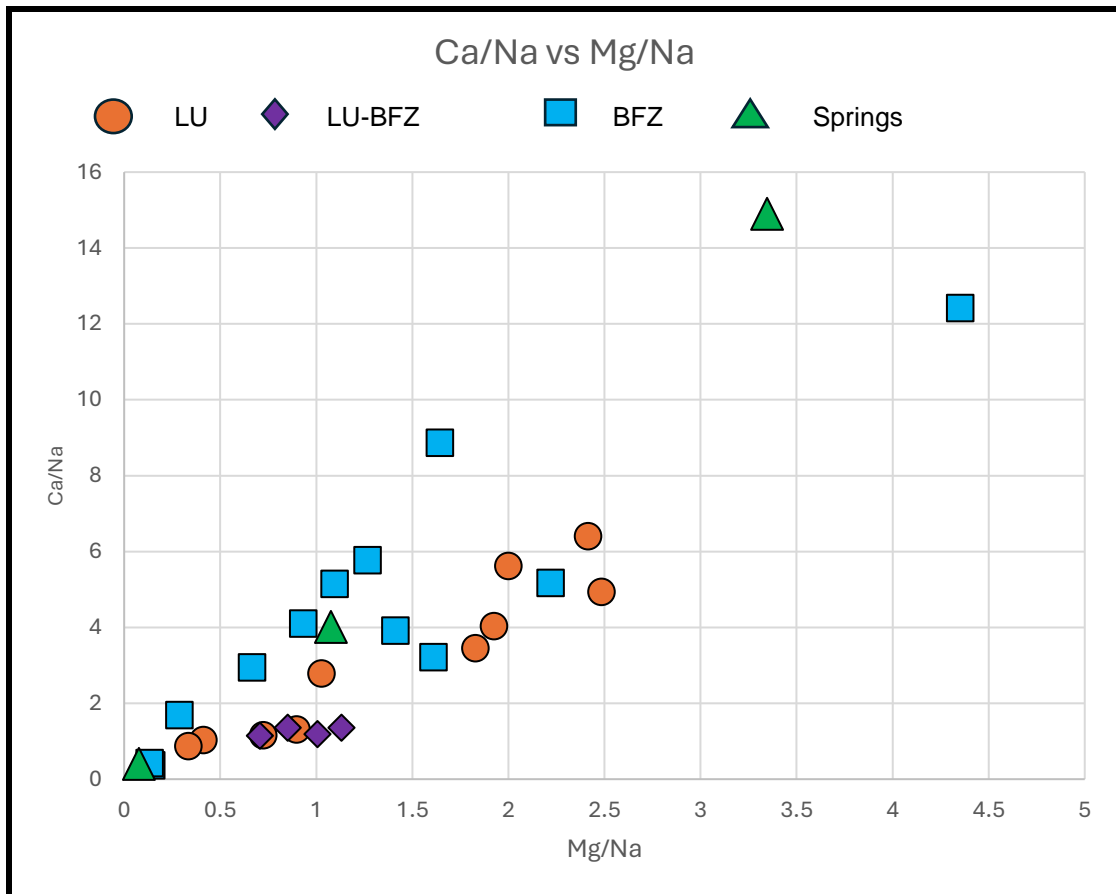


Figure 13: Major element ratio plot with different sample types. Llano Uplift (orange circle), in-between LU and BFZ (purple diamond), Balcones fault zone (blue square), and springs (green triangle).

5.7. Trends in Sr and U isotope vs. concentrations

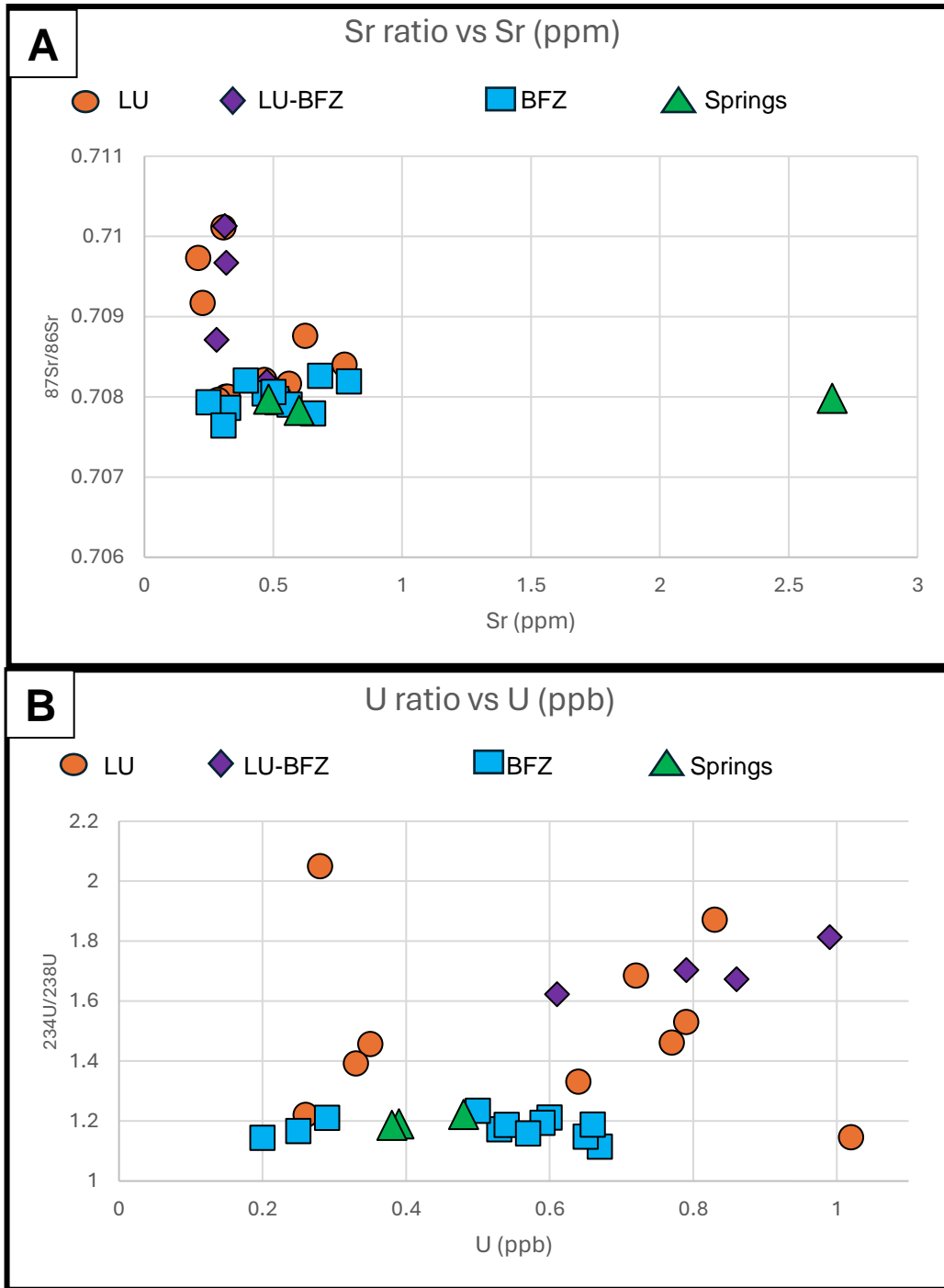


Figure 14: (A) Sr ratio vs Sr (ppm) and (B) U ratio vs U (ppb) plots. Llano Uplift (orange circle), in-between LU and BFZ (purple diamond), Balcones fault zone (blue square), and springs (green triangle).

Figure 14A is a plot of $^{87}\text{Sr}/^{86}\text{Sr}$ vs Sr (ppm), showing distinct regions. All four sample groups have samples that plot within a similar region around 0.5 ppm Sr and 0.708 $^{87}\text{Sr}/^{86}\text{Sr}$. All BFZ samples cluster in this region. LU and LU-BFZ samples create a linear spread to higher $^{87}\text{Sr}/^{86}\text{Sr}$ ratios. Two of the spring samples also plot within this region, although a single anomalous sample contains elevated Sr compared to any other sample in the study.

Trends in U are also highlighted by each group of samples, although together the entire dataset is complex (Fig. 14B). BFZ samples form a near horizontal array at low $^{234}\text{U}/^{238}\text{U}$ values across a range of U ppm. Spring samples are similar, but with a more restricted range in U ppm. LU and LU-BFZ samples are more scattered. In the LU samples $^{234}\text{U}/^{238}\text{U}$ ranges from ~ 1.0 to ~ 2.0 and U varies from ~ 0.26 ppb to ~ 1.0 ppb with no clear trend. LU-BFZ samples show a slight positive trend at elevated $^{234}\text{U}/^{238}\text{U}$ and U values.

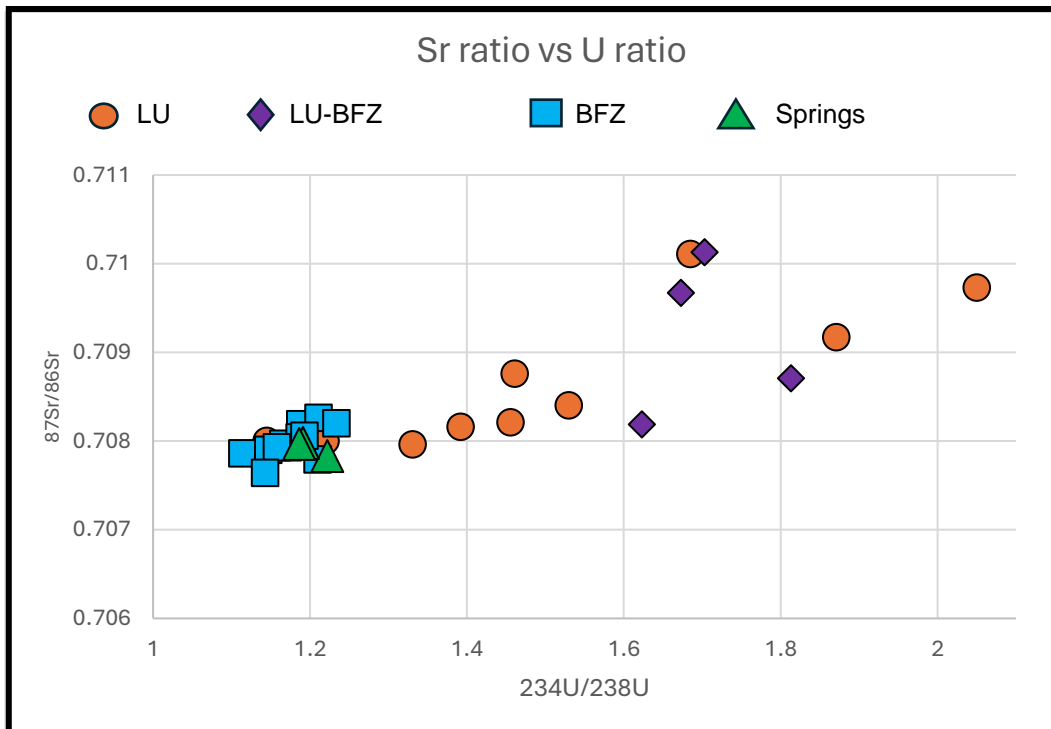


Figure 15: Sr vs U ratio plot with different sample types. Llano Uplift (orange circle), in-between LU and BFZ (purple diamond), Balcones fault zone (blue square), and springs (green triangle).

Figure 15 displays $^{234}\text{U}/^{238}\text{U}$ plotted against $^{87}\text{Sr}/^{86}\text{Sr}$. Overall, the entire dataset shows a positive correlation between $^{234}\text{U}/^{238}\text{U}$ and $^{87}\text{Sr}/^{86}\text{Sr}$, with important distinctions between each region. The LU samples show a linear positive trend, with $^{87}\text{Sr}/^{86}\text{Sr}$ ratio ranging from ~ 0.708 to ~ 0.71011 , and $^{234}\text{U}/^{238}\text{U}$ ratio varying from ~ 1.145 to ~ 2.05 . In contrast, the BF and springs samples show little variation and are more concentrated around Sr ratio ~ 0.708 and U ratio ~ 1.15 . The LU-BFZ samples display a slightly scattered pattern, with Sr ratio ranging from ~ 0.708 to 0.71013 and U ratio varying from ~ 1.62 to ~ 1.8 .

CHAPTER 6: DISCUSSIONS

6.1. Endmember Lithologies Affect Downstream River Chemistry

In Figure 16, plots of all samples from this study are displayed alongside a global compilation of the largest rivers from Gaillardet and colleagues (1999). This study's samples exhibit similar trends to the global dataset. Samples within the Llano Uplift and in-between LU and BFZ (dark blue and dark green circles) appear to show mixing between silicates and carbonate lithologies. These mixings likely result from the Colorado River and its tributaries traversing through Lower Paleozoic and Lower Cretaceous formations, where carbonate is the predominant lithology, before entering Proterozoic metamorphic and igneous rocks.

Additionally, samples located immediately downstream of the Llano Uplift plot almost within the silicate field. These samples, from the Pedernales and Colorado rivers (LU11, LU12, LU13, and LU14), are situated on the outer edge of the Llano Uplift and transitioning into carbonate lithology.

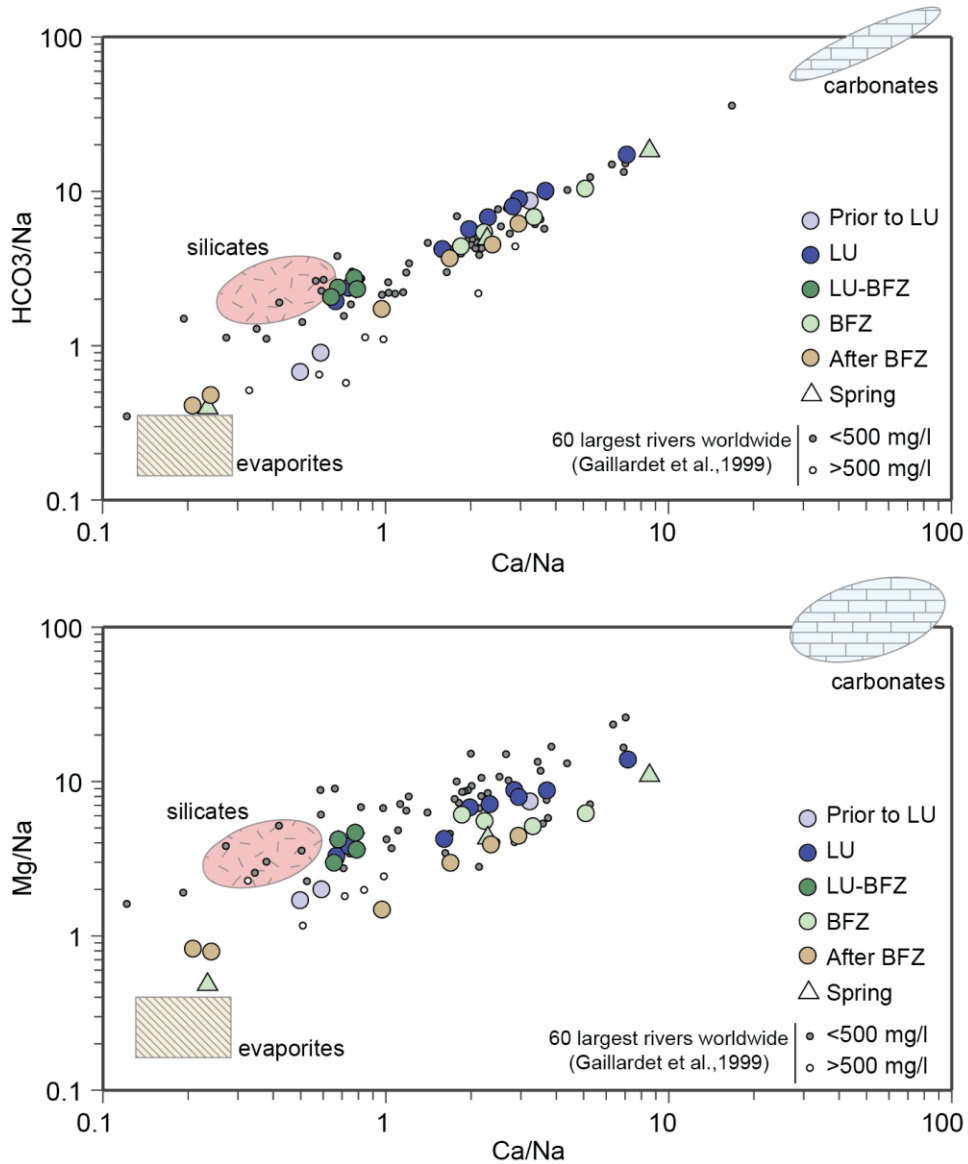


Figure 16: Mixing diagrams using Na-normalized molar ratio element in the study area plotted with 60 largest rivers from Gaillardet et al., (1999) with rivers having TDS values greater than 500 mg l⁻¹ (open circles). Study area samples are modified to prior to LU (light blue circle), within the LU (dark blue circle), in-between LU and BFZ (dark green circle), within the BFZ (light green circle), after BFZ (brown circle), and springs (triangle).

The samples downstream of the BFZ (brown circles) exhibit mixing between evaporites and carbonates with minor silicate input, along with the spring sample (triangle) plotting close to the evaporites field. These samples are from the San Antonio River (BF5 and BF6) and San Pedro Springs Pool (BF4). The San Pedro Springs Pool sample is located in Upper Cretaceous formations composed of carbonate, while the San Antonio samples are situated in Cenozoic

sediments. The presence of evaporite signatures could possibly be attributed to fluids at depth that flow through the Glen Rose Formation in the Lower Cretaceous units and move to the surface through fault conduits. These observations further support the interpretation that lithology is a major control on river water chemistry.

6.2. Bicarbonate (HCO₃)

In the upstream areas of the Colorado River, HCO₃ concentrations seem to be influenced by lithology (Fig. 8). Initially, in silicate areas, values are relatively low, around 120 ppm, then rise to 266 ppm upon encountering carbonate bedrock. As the river approaches the Llano Uplift, HCO₃ levels decrease to approximately ~183 ppm. However, downstream within the BFZ, where carbonate bedrock predominates, concentrations increase again to around ~190 ppm. Among the Colorado River tributaries, the San Saba River demonstrates a similar trend. Originating from carbonate rocks with levels around 280 ppm, concentrations decrease to approximately 231 ppm upon reaching the Llano Uplift before merging with the Colorado River at approximately 266 ppm. Similarly, the Llano River exhibits a decrease from around 233 ppm on carbonate rocks to about 184 ppm within the uplift, merging with the Colorado River at approximately 183 ppm. Conversely, the Pedernales River shows an increasing trend, starting around 193 ppm on carbonate rocks and rising to about 240 ppm before merging with the Colorado River at approximately 185 ppm. These observations suggest significant lithological influences on HCO₃ concentrations in both the Llano Uplift and downstream into the BFZ.

Moreover, samples from the BFZ indicate fault-related influences on HCO₃. For instance, the Medina River, a tributary to the San Antonio River, experiences an increase in HCO₃ concentrations from 246 to approximately 305 ppm downstream across the BFZ before merging with the San Antonio River. Similarly, the San Pedro Springs, which feed the San

Antonio River, exhibit low HCO_3^- ~163 ppm, increasing downstream to 260 ppm before slightly decreasing to 250 ppm in Cenozoic sediments. The Guadalupe River starts with relatively high values of around 264 ppm on carbonate rocks, decreasing slightly to about 258 ppm at the outer part of the BFZ, and significantly dropping to around 149 ppm downstream across the BFZ. However, concentrations increase again to approximately 212 ppm upon reaching Cenozoic sediments. Likewise, the San Marcos River demonstrates a decreasing trend despite originating from carbonate rocks, with concentrations starting at approximately 344 ppm and decreasing downstream to about 312 ppm on Cenozoic sediments before further decreasing to around 200 ppm. Notably, Barton Springs and Jacob's Well both exhibits relatively high values of around 330 and 354 ppm, respectively. In contrast, the San Pedro Spring Pool, located at the outer edge of the BFZ where carbonate rocks transition to Cenozoic sediments, displays a significantly lower value of 163 ppm. Additionally, downstream of the San Antonio River, HCO_3^- concentrations increase to around 255 ppm, much higher than other downstream of BFZ samples, possibly influenced by evaporite signatures as previously mentioned. Altogether, these variations in HCO_3^- concentrations suggest possible influences from both lithology and faults within the BFZ.

6.3. Lithologic Controls on Sr and U

The upstream samples for LU exhibit a relatively high Sr ratio of 0.70973 and a U ratio of 2.05 in the Upper Paleozoic formations, including carbonate and silicate regions, and minor evaporites upstream of the Colorado River (see Figs. 1A, 9, and 10). As the Colorado River flows downstream towards the Llano Uplift, both Sr and U ratios increase. This trend persists in the San Saba, Llano, and Pedernales rivers, which exhibit similar increases in Sr and U ratios before merging with the Colorado River, despite being situated in Lower Cretaceous formations

primarily consisting of carbonate deposits. As these rivers traverse the Llano Uplift, characterized by predominantly Proterozoic rocks such as gneiss, schists, and granite, both Sr and U ratios experience a significant increase. The highest Sr ratio observed is 0.71011, accompanied by a high U ratio of 1.871. Similarly, the LU-BFZ samples display Sr ratios ranging from 0.70871 to 0.71013 and U ratios ranging from 1.623 to 1.813. Eventually, as the Colorado River exits the Llano Uplift and approaches the Balcones fault zone, both Sr and U ratios decrease as the river flows through carbonate rocks.

Continuing downstream into the BFZ, where the lithology predominantly comprises carbonates from the Lower Cretaceous formations, both Sr and U ratios dramatically decrease. For instance, at the Barton Spring Pool, a tributary to the Colorado River, the Sr ratio drops to 0.70798, with U ratio of 1.191. Conversely, BFZ samples exhibit minimal fluctuations in both Sr and U ratios, with values ranging from 0.70764 to 0.70826 for Sr and 1.114 to 1.234 for U, excluding exceptions such as the Medina River a tributary of the San Antonio River, which experiences a slight increase in Sr and U ratios as the lithology transitions from Lower Cretaceous carbonate to Cenozoic sediments. Analysis of the San Antonio River reveals a clear transition from the San Pedro Spring pool to downstream, exhibiting Sr and U ratios of 0.70797 and 1.186. This trend continues as the river flows southeast into Cenozoic sediments, showing slight increases in Sr and U ratios. Similar observations are made with the Guadalupe and San Marcos rivers.

Furthermore, spring samples located in the Lower Cretaceous formations exhibit values similar to nearby rivers, except for the Jacob's Well, which demonstrates a slightly higher U ratio of 1.222. This discrepancy may be attributed to variations in U concentration (ppb), which

also tends to be higher at Jacob's Well compared to other spring samples, suggesting a correlation between U concentration and U ratio in spring samples.

These U ratio values in surface water closely resemble those reported by Kronfeld (1974), ranging from approximately 1.23 to 1.42 in the Austin, TX area. Similarly, Sr ratio values are slightly higher than those reported for carbonate rocks in the Edwards Aquifer by Oetting et al. (1994), range of 0.7074 to 0.7076. The Sr ratio values relatively reflect the values found in Bataille & Bowen (2012) as seen in Figure 4. Overall, correlation of Sr and U values with differences in rock type suggests that lithology has a major influence on Sr and U values.

6.4. Vertical and Structural Controls on Electrical Conductivity

Unlike Sr and U isotopes ratios, lateral variation in lithology appears to have little influence on the electrical conductivity (EC) values throughout the study area, although some notable exceptions are observed. Relatively low EC values are found in the vicinity of the Llano Uplift, averaging around 450 $\mu\text{s}/\text{cm}$ while the majority of EC ranging from ~ 530 to ~ 720 $\mu\text{s}/\text{cm}$ (Fig. 7).

However, spring samples exhibit significantly higher EC levels, ranging from approximately 797 $\mu\text{s}/\text{cm}$ at Jacob's Well to a high of 1005 $\mu\text{s}/\text{cm}$ at San Pedro Springs. Moreover, in the case of the San Antonio River, EC values are elevated in areas characterized by Cenozoic sediments, reaching up to approximately 1728 $\mu\text{s}/\text{cm}$, before decreasing to 1476 $\mu\text{s}/\text{cm}$ downstream. A similar trend is observed in the San Marcos River, which is spring-fed and exhibits high EC values of around 822 $\mu\text{s}/\text{cm}$, decreasing downstream to approximately 530 $\mu\text{s}/\text{cm}$.

System	Provincial series	Group	Formation	Function	Member or Informal unit	Function	Thickness (feet)	Lithology	Hydrostratigraphy
Cretaceous	Comanchean	Trinity	Glen Rose	CB	Upper part of Glen Rose	CB	300-400	Limestone, dolomite, shale and marl. Alternating beds of carbonates and marls. Evaporites and dolomites toward top variable bedding.	Supratidal and shoreline deposits toward top. Tidal to subtidal deposits below. Unit has little vertical permeability but has moderate lateral permeability.
				AQ	Lower part of Glen Rose	AQ	200-250	Massive limestone with few thin beds of marl.	Marine deposits - caprinid reef zones and porous and permeable honeycomb porosity near the base.
			Pearsall (Travis Peak in outcrop)	CB	Bexar	CB	300	Limestone and shale.	Shoreline deposits, relatively impermeable unit in the Balcones fault zone.
				AQ	Cow Creek Limestone member	AQ		Limestone and dolomite. Grainstone, packstone, and coquinoid beds.	Moderately permeable unit in Comal County.
				CB	Pine Island Shale member	CB		Shale and argillaceous limestone.	Little permeability.
Coahuilan	Nuevo Leon and Durango of Mexico	Sligo and Hosston Formations	CB			800-1,500	Limestone, shale, and sandstone.	Sandstone in lower part is moderately permeable.	
Pre-Cretaceous							Slate, phyllite, locally sedimentary rocks in grabens.	Basement rocks. No circulating ground water.	

Figure 17: Modified table from Maclay and Small (1984) summary of the lithology and water-bearing characteristic on the San Marcos Platform in the Balcones fault zone.

Both the San Marcos and San Antonio rivers, predominantly spring-fed and situated on the BFZ, likely experience varying influences from groundwater. The exceptionally high EC value observed in the San Antonio River could be attributed to elevated levels of total dissolved solids (TDS), whereas the San Marcos River may exhibit lower TDS concentrations (see Figure 18). The groundwater flow dynamics in the region may contribute to the differences in TDS levels, especially at these two rivers. The fault system at the San Antonio River area, possibly extending to deeper depths within the Lower Cretaceous formations, is likely a significant factor. This depth allows groundwater to interact with various formations, such as the Glen Rose Formation, potentially picking up dissolved evaporites that contribute to the observed EC values and slightly elevated Sr ratio (see Figs. 6B and 17). Further investigation into these groundwater dynamics is warranted to fully understand their impact on EC values in the BFZ.

6.5. The Influence of Geologic Structure on River Chemistry

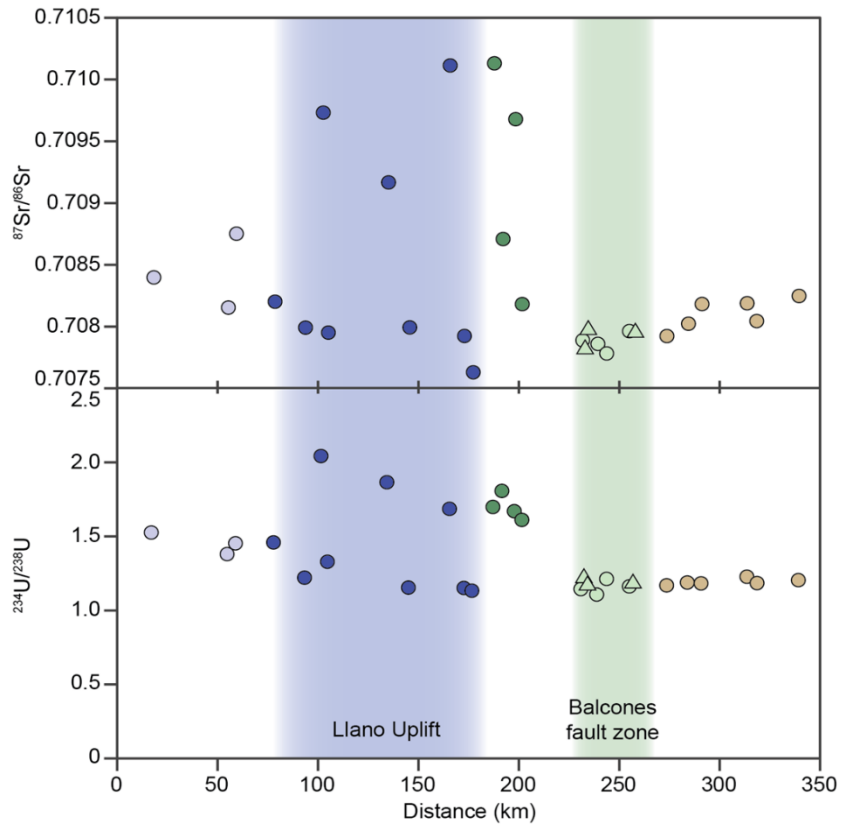


Figure 19: Plot of Sr and U ratio vs distance of the Llano Uplift (blue region) and Balcones fault zone (green region).

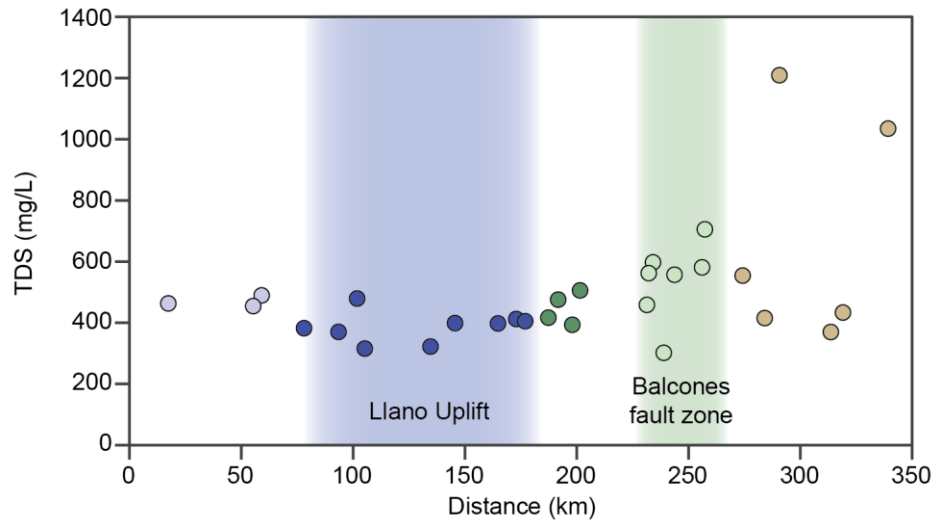


Figure 18: Plot total dissolved solids (TDS) in mg/L vs distance of the Llano Uplift (blue region) and Balcones fault zone (green region).

6.5.1. Llano Uplift

The Llano Uplift does appear to influence the surface water chemistry. This influence becomes apparent when considering the lithological composition of the Llano Uplift being mostly Proterozoic gneiss, schists, and granite, which emerges as the primary factor influencing the Sr and U ratio as seen in Figures 9 and 10. These figures depict a clear trend wherein both Sr and U ratio show noticeable increase as the river approaches the vicinity of and within the Llano Uplift e.g., the Colorado and Llano rivers. In addition, Figure 18 shows elevated Sr and U ratio within the Llano Uplift region, with Sr ratio reaching high as ~ 0.710 and U ratio ~ 2.0 , followed by a subsequent decrease as distance from the Llano Uplift increases.

In contrast, the Llano Uplift does not appear to significantly influence the electrical conductivity (EC) as seen in Figure 7. Apart from having a relatively low EC of $\sim 450 \mu\text{s}/\text{cm}$ within the Llano Uplift, the EC for samples in the vicinity of the Llano Uplift show a slight increase in EC of $\sim 550 \mu\text{s}/\text{cm}$.

Moreover, the bicarbonate concentrations (Fig. 8) also reflect some influence from the Llano Uplift, with relatively low concentrations ranging from ~ 180 to ~ 200 ppm on Proterozoic rocks compared to higher concentrations of ~ 260 to ~ 280 ppm on Paleozoic and Mesozoic carbonate rocks. The lower concentration in Proterozoic rocks is likely due to their composition of hard rocks such as gneiss, schists, and granite, which are more resistant to weathering. In contrast, Paleozoic and Mesozoic carbonate rocks are relatively softer and easier to weather, which can introduce more particles into the river system, resulting in higher bicarbonate concentrations. Altogether, the lithological composition of the Llano Uplift significantly impacts surface water chemistry, as evidenced by the observed variations in Sr and U ratios, as well as bicarbonate concentrations.

6.5.2. Balcones Fault Zone

The BFZ zone does appear to have a minor influence on surface water chemistry. This influence is not driven by lateral changes in rock lithology, but by vertical conduits which introduce deeper waters into the river systems. In Figures 9 and 10, the Sr and U ratios over the BFZ show consistency, with Sr ratio averages from around ~0.707 to ~0.708 and U ratio averages from around ~1.1 to ~1.2. Additionally, the U ratio is relatively higher in springs sample such as in the Jacob's Well (BF14) and Barton Spring Pool (BF15). These slight elevated U ratios are likely due to the fault system acting as conduit for fluids from deeper depth to flow through and influence the springs water chemistry by introducing excess ^{234}U into the hydrological system (Fig. 5B). In addition, Figure 18 shows very little impact, and shows lower values for Sr and U ratio over the distance to the BFZ.

Additionally, the BFZ does appear to have an influence on the electrical conductivity (EC). The recorded EC values within the BFZ averaging around ~650 to 850 $\mu\text{s}/\text{cm}$, with the lowest recorded at the Jacob's Well 428 $\mu\text{s}/\text{cm}$ (BF14) and the highest recorded at the San Pedro Spring Pool 1005 $\mu\text{s}/\text{cm}$ (BF4). These average values likely stem from the presence of excess total dissolved solids (TDS) within the hydrologic system in the subsurface that was transferred to and mixed with surface water through fault conduits (Fig. 5-B and 18).

Moreover, the bicarbonate concentrations (Fig. 8) reflect some influence from the BFZ. Some of the highest values are along within the BFZ averaging around ~305 to ~350 ppm, with some of the lowest values are from one sample in the Guadalupe River 149 ppm (BF12) and the San Pedro Spring Pool 163 ppm (BF4). These average values are likely due to the slight increase in salinity from water at depth that was transferred to and mixed with surface water through fault conduits.

Altogether, the BFZ has a lesser impact on the Sr and U ratios. However, both recorded EC and bicarbonate values show a greater influence from the BFZ. This influence is likely attributed to the transfer of fluids from depth through the fault system which subsequently mixed with surface water. These fluids then introduce excess total dissolved solids (TDS) resulting in high EC, and fluids that are slightly elevated in salinity resulted in the increased in bicarbonate concentrations.

6.6. Schematic conceptual model of surface water chemistry changes in Central Texas

In summary, this study highlights the critical importance of understanding the hydrogeological dynamics of large geologic structures such as the Llano Uplift and the BFZ and influences on surface water chemistry. Figure 20 presents a comprehensive overview of the research, illustrating how a river's water chemistry changes as it flows through different lithology and structures. When the river traverses through Paleozoic and Mesozoic carbonate rocks, there's a notable increase in EC due to the rocks' susceptibility to weathering. In contrast, Proterozoic crystalline rocks are more resistant to weathering, resulting in lower EC levels. This weathering of carbonate rocks leads to elevated TDS concentrations in the water, consequently elevating EC levels. Similarly, bicarbonate (HCO_3) concentrations tend to rise in carbonate rocks and decline in crystalline rocks. Moreover, when the river crosses the BFZ, EC and HCO_3 levels increase due to groundwater influences via fault conduits, introducing additional TDS and

HCO₃ into surface water. However, as the river moves away from carbonate rocks and the BFZ into regions with unconsolidated sediments, EC and HCO₃ concentrations gradually decrease.

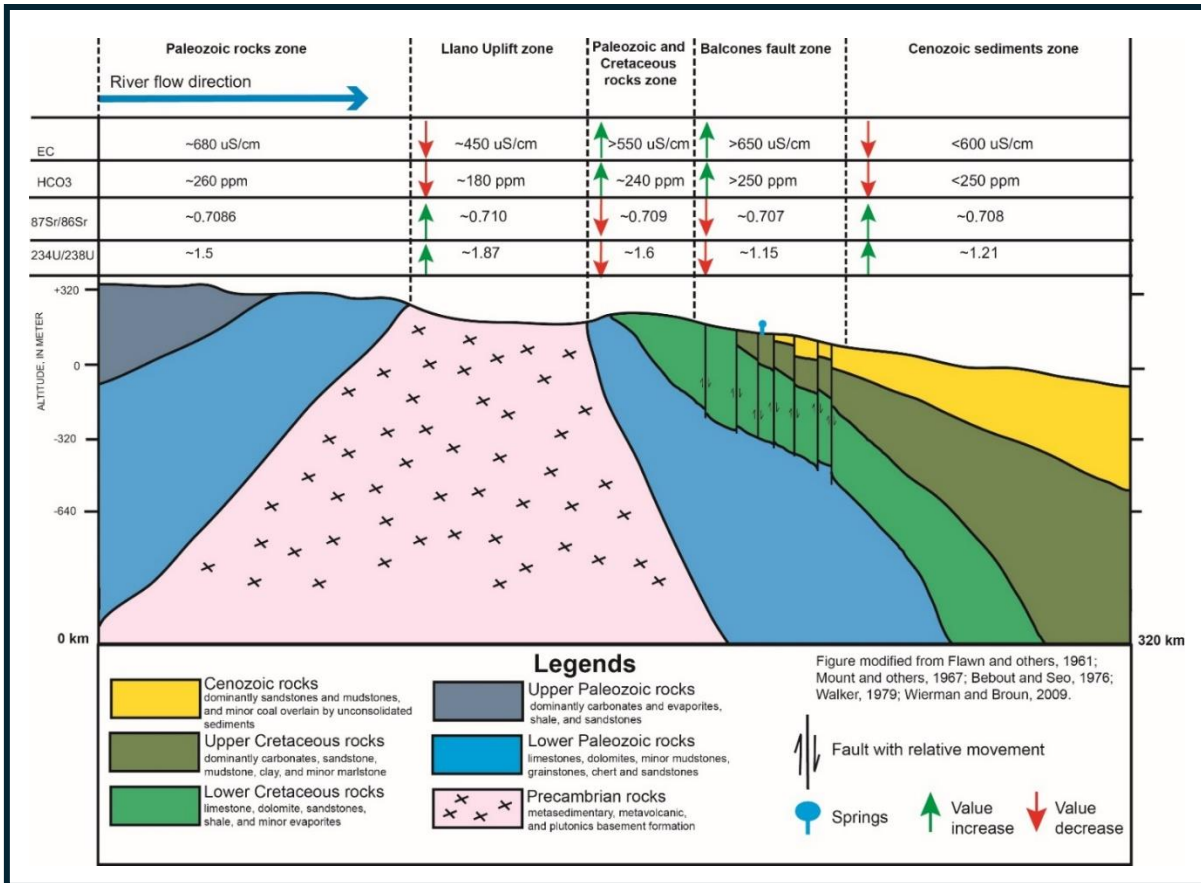


Figure 20: Cross-sectional schematic model illustrating the influence of lithology and structure on surface water chemistry.

Furthermore, Sr and U ratios dramatically increase when the river is flowing over the Llano Uplift, this is due to the lithologies making up of Proterozoic age crystalline rocks such as gneiss, schists, and granite. The elevated ratios are the result of the prolonged evolution of strontium ratios over time, a consequence of Rb/Sr fractionation and uranium decaying in granitic rocks. Both Sr and U ratios dramatically decrease as the river flows out of the Llano Uplift and into carbonate regions where the surface water chemistry gets diluted from carbonate rocks. Moreover, Sr and U ratios further decrease on the BFZ due to surface water further mixing

with groundwater from underlying carbonate aquifers and lithology. Upon leaving carbonate rocks and the BFZ, entering region with unconsolidated sediments, Sr and U ratios experience a slight increase as surface water ceases to mix with groundwater.

CHAPTER 7: CONCLUSION

In conclusion, this study demonstrates that the Llano Uplift and the BFZ significantly influences surface water chemistry, particularly evident in the variations observed in strontium and uranium isotopes ratios. The elevated isotopic ratios are notably observed over Proterozoic crystalline rocks, contrasting with decreased ratios in Paleozoic and Mesozoic rocks. Changes in EC and HCO₃ concentrations across different lithologies were less pronounced. Conversely, the BFZ exerts more influence on EC and HCO₃ concentrations than on strontium and uranium isotopes.

These findings provide valuable insights for managing water resources, predicting groundwater movement, and mitigating contamination risks. Given the essential role of surface water in meeting societal needs across various sectors, including drinking water supply, agriculture, industry, and ecosystem health, therefore understanding the influence of geological structures and lithology on surface water chemistry is paramount. This knowledge not only enriches our understanding of local hydrogeological systems but also provides a robust framework for implementing effective measures to safeguard water quality and availability. Continued research in this field will further refine our knowledge and enable more effective measures for safeguarding water quality and availability in the region and beyond.

REFERENCES

- Abbott, P. L., & Woodruff, C. M. (1986). The Balcones Escarpment: Geology, hydrology, ecology and Social Development in Central Texas. Geological Society of America Annual Meeting. Abbott, P., & Woodruff, C. M. Jr. (1986). The Balcones Escarpment. 1986, 212.
- Barker, R.A., and Ardis, A.F., 1996, Hydrogeologic framework of the Edwards-Trinity aquifer system, west-central Texas: U.S. Geological Survey Professional Paper 1421-B, 61 p.
- Bataille, C. P., & Bowen, G. J. (2012). Mapping $^{87}\text{Sr}/^{86}\text{Sr}$ variations in bedrock and water for large scale provenance studies. *Chemical Geology*, 304–305, 39–52.
<https://doi.org/10.1016/j.chemgeo.2012.01.028>
- Bullen, T.D., Krabbenhoft, D.P. & Kendall, C., 1996, Kinetic and mineralogic controls on the evolution of groundwater chemistry and $^{87}\text{Sr}/^{86}\text{Sr}$ in a sandy silicate aquifer, northern Wisconsin, USA: *Geochimica et Cosmochimica Acta*, v. 60, p. 1807-1821.
- Burke, W. H., Denison, R. E., Hetherington, E. A., Koepnick, R. B., Nelson, H. F., & Otto, J. B. (1982). Variation of seawater $^{87}\text{Sr}/^{86}\text{Sr}$ throughout Phanerozoic time. *Geology*, 10(10), 516-519.
- Capo, R.C., Stewart, B.W., Chadwick, O.A., 1998. Strontium isotopes as tracers of ecosystem processes: theory and methods. *Geoderma* 82(1), 197–225. [https://doi.org/10.1016/S0016-7061\(97\)00102-X](https://doi.org/10.1016/S0016-7061(97)00102-X)

- Carlson, W. D., 1998, Petrologic constraints on the tectonic evolution of the Llano Uplift, in Gilbert, M. C., and Hogan, J. P., eds., *Basement tectonics 12*: Dordrecht, Netherlands, Kluwer Academic Press, p. 3–27.
- Chabaux F., A.S. Cohen, R.K. O’Nions, and J.R. Hein, 1995, ^{238}U - ^{234}U - ^{230}Th chronometry of Fe- Mn crusts. *Geochimica et Cosmochimica Acta* 59, 633–638.
- Chabaux, F., Riotte, J., & Dequincey, O. (2003). U-Th-Ra fractionation during weathering and river transport. In: Bourdon, B., Henderson, G.M., Lundstrom, C.C., Turner, S.P. (Eds.), *Uranium-Series Geochemistry*. *Rev. Mineral. Geochem.* 52, 533–576.
- Chabaux, F., Bourdon, B., Riotte, J., 2008. U-series geochemistry in weathering profiles, river waters and lakes. *Radioact. Environ.* 13, 49–104.
- Cheng, H., Edwards, R.L., Hoff, J., Gallup, C.D., Richards, D.A., Asmerom, Y., 2000. The half-lives of uranium-234 and thorium-230. *Chem. Geol.* 169, 17–33.
- Clark, D. L., Hobart, D. E., & Neu, M. P. (1995). Actinide Carbonyl Complexes and Their Importance in Actinide Environmental Chemistry. *Chemical Reviews*, 95(1), 25–48.
<https://doi.org/10.1021/cr00033a002>
- Collins, E. W. (1993). Fracture Zones between Overlapping En Echelon Fault Strands: Outcrop Analogs within the Balcones Fault Zone, Central Texas. 1993, 43, 77–85.
- Collins, E. W., and Hovorka, S. D., (1997), Structure Map of the San Antonio Segment of the Edwards Aquifer and Balcones Fault Zone, South-Central Texas: Structural Framework of a Major Limestone Aquifer: Kinney, Uvalde, Bexar, Comal, and Hays Counties: The

University of Texas at Austin, Bureau of Economic Geology, Miscellaneous Map No. 38, map scale 1:250,000, and 14-page booklet.

Crossey, L. J., Fischer, T. P., Patchett, P. J., Karlstrom, K. E., Hilton, D. R., Huntoon, P., & Reynolds, A. C. (2006). Dissected hydrologic system at Grand Canyon: Interaction between upper world and lower world waters in modern springs and travertine. *Geology*, 34, 25-28.

Davidson, A., 1986, New interpretation of the southwestern Grenville Province, in Moore, J. M., Jr., Davidson, A., and Baer, A. J., eds., *The Grenville province: Geological Association of Canada Special Paper 31*, p. 61–74.

Drever, J.I., 1997, *The Geochemistry of Natural Waters: Surface and Groundwater Environments*, [ISBN-10: 0132727900].

Ewing, T. E. (2005). Phanerozoic Development of the Llano Uplift. 45(9), 15-25.

Ferrill, D.A., Morris, A.P., and McGinnis, R.N., (2019), Geologic structure of the Edwards (Balcones Fault Zone) Aquifer. In *The Edwards Aquifer: The Past, Present, and Future of a Vital Water Resource* (eds JM Sharp Jr, RT Green and GM Schindel), pp. 171–88. Geological Society of America Memoir no. 215.

Flawn, P. T., Goldstein, A., Jr., King, P. B., and Weaver, C. E., (1961), *The Ouachita System*: University of Texas, Austin, Bureau of Economic Geology Publication 6120, 401 p.

Flawn, P. T., and Muehlberger, W. R., 1970, The Precambrian of the United States of America; South-Central United States, in Rankama, K. (ed.), *The Geologic Systems, The Precambrian*: Interscience, v. 4, p. 72-143.

- Fleischer, R.L., 1980. Isotopic disequilibrium of uranium: alpha-recoil damage and preferential solution effects. *Science* 207, 979–981.
- Gaillardet, J., Dupré, B., Louvat, P., & Allègre, C. J. (1999). Global silicate weathering and CO₂ consumption rates deduced from the chemistry of large rivers. *Chemical Geology*, 159(1–4), 3–30. [https://doi.org/10.1016/S0009-2541\(99\)00031-5](https://doi.org/10.1016/S0009-2541(99)00031-5)
- Goff, F., Evans, W. C., Gardner, J. N., Adams, A., & Janik, C. J. (1994). Interpretation of in-situ fluid samples from geothermal wells: Example from hole VC-2B, Valles caldera, New Mexico. *Geothermal Science and Technology*, 4(2), 97-128.
- Grabowski, P., & Bem, H. (2012). Uranium isotopes as a tracer of groundwater transport studies. *Journal of radioanalytical and nuclear chemistry*, 292(3), 1043–1048. <https://doi.org/10.1007/s10967-011-1558-0>
- Hynes, A., & Rivers, T. (2010). Protracted continental collision — evidence from the Grenville Orogen. *Canadian Journal of Earth Sciences*, 47(5), 591–620. doi:10.1139/e10-003
- Kirkland, D. W., Denison, R. E., & Evans, R. (1995). Middle Jurassic Todilto Formation of Northern New Mexico and Southwestern Colorado: Marine or Nonmarine? *New Mexico Bureau of Mines and Mineral Resources Bulletin*, 147, 37.
- Konter, J.G., Storm, L.P., 2014. High precision ⁸⁷Sr/⁸⁶Sr measurements by MC-ICP-MS, simultaneously solving for Kr interferences and mass-based fractionation. *Chem. Geol.* 385, 26–34. <https://doi.org/10.1016/j.chemgeo.2014.07.009>.

- Kronfeld, J. (1974). Uranium deposition and Th-234 alpha-recoil: An explanation for extreme U-234/U-238 fractionation within the trinity aquifer. *Earth and Planetary Science Letters*, 21(3), 327-330. [https://doi.org/10.1016/0012-821X\(74\)90169-1](https://doi.org/10.1016/0012-821X(74)90169-1)
- Kronfeld, J., Vogel, J. C., & Talma, A. S. (1994). A new explanation for extreme ^{234u}/^{238u} disequilibria in a dolomitic aquifer. *Earth and Planetary Science Letters*, 123(1-3), 81-93.
- Langmuir, D. (1978). Uranium solution–mineral equilibria at low temperatures with applications to sedimentary ore deposits. *Geochimica et Cosmochimica Acta*, 42, 547–569.
- Lindgren, R.J., Dutton, A.R., Hovorka, S.D., Worthington, S.R.H., and Painter, S., (2004), Conceptualization and simulation of the Edwards aquifer, San Antonio region, Texas: U.S. Geological Survey Scientific Investigations Report 2004–5277, 143 p.
- Ma L., Chabaux F., Pelt E., Blaes E., Jin L. and Brantley S. L. (2010) Regolith production rates calculated with uranium-series isotopes at Susquehanna/Shale Hills Critical Zone Observatory. *Earth Planet. Sci. Lett.* 297, 211–225.
- Maclay, R. W., & Small, T. A. (1984). Carbonate geology and hydrology of the Edwards Aquifer in the San Antonio area, Texas. USGS Numbered Series 83–537; Open-File Report, p. 72. U.S. Geological Survey. <https://doi.org/10.3133/ofr83537>
- McArthur, J. M., Howarth, R. J., & Bailey, T. R. (2001). Strontium isotope stratigraphy: LOWESS Version 3: Best fit to the marine Sr isotope curve for 0-509 Ma and accompanying look-up table for deriving numerical age. *Journal of Geology*, 109, 155-170. <https://doi.org/10.1086/319243>

- Mosher, S., (1993). Western extensions of Grenville age Rocks, Texas, in Reed, J. C., Jr., Bickford, M. R. E., Houston
- Mosher, S. (1998). Tectonic evolution of the southern Laurentian Grenville orogenic belt. Geological Society of America Bulletin, 110(11), 1357-1375.
[https://doi.org/10.1130/0016-7606\(1998\)110<1357:TEOTSL>2.3.CO;2](https://doi.org/10.1130/0016-7606(1998)110<1357:TEOTSL>2.3.CO;2)
- Muehlberger, W. R., Denison, R. E., and Lidiak, E. G., 1967, Basement rocks in the continental interior of the United States: American Association of Petroleum Geologists Bulletin, v. 12, p. 2351-2380.
- Mukhopadhyay, B., & Brookins, D. G. (1976). Strontium isotopic composition of the Madera Formation (Pennsylvanian) near Albuquerque, New Mexico. *Geochimica et Cosmochimica Acta*, 40(6), 611-616.
- Murphy, W.M., Shock, E.L., 1999. Environmental aqueous geochemistry of actinides. In: Burns, P.C., Finch, R. (Eds.), *Uranium: Mineralogy, Geochemistry, and the Environment*, Rev. Mineral. Geochem. 38, 221–253 p.
- Murray, G.E., (1961) *Geology of the Atlantic and Gulf Coastal Province of North America*. New York: Harper and Brothers, 692 pp.
- Oetting, G.C., Banner, J.L., and Sharp, J.M., Jr., (1994), Regional geochemical and isotopic variations in bad- waters of the Edwards aquifer, in *Edwards aquifer field trip guidebook Toxic Substances and the Hydrologic Sciences Conference*, Austin, Tex., April 10–13, 1994: American Institute of Hydrology, p. 1–13.

Paces, J. B., & Wurster, F. C. (2014). Natural uranium and strontium isotope tracers of water sources and surface water-groundwater interactions in arid wetlands - Pahranaagat Valley, Nevada, USA. *Journal of Hydrology*, 517, 213-225.

<https://doi.org/10.1016/j.jhydrol.2014.05.011>

Porcelli, D., Swarzenski, P.W., 2003. The behavior of U- and Th-series nuclides in groundwater. In: Bourdon, B., Henderson, G.M., Lundstrom, C.C., Turner, S.P. (Eds.), *Uranium-Series Geochemistry*. *Rev. Mineral. Geochem.* 52, 317-361.

Walker, N. (1992). Middle Proterozoic geologic evolution of Llano uplift, Texas: Evidence from U-Pb zircon geochronometry. *Geological Society of America Bulletin*, 104(4), 494-504.

[https://doi.org/10.1130/0016-7606\(1992\)104<0494:MPGEOL>2.3.CO;2](https://doi.org/10.1130/0016-7606(1992)104<0494:MPGEOL>2.3.CO;2)

Reese, J. F., 1995, Structural evolution and geochronology of the southeastern Llano Uplift, central Texas. [Ph.D. dissert.]: Austin, University of Texas at Austin, 172 p.

Rivers, T., Martignole, J., Gower, C. F., and Davidson, A., 1989, New tectonic divisions of the Grenville Province, southeast Canadian shield: *Tectonics*, v. 8, p. 63-84.

Roback, R. C., 1996, Characterization and tectonic evolution of a Mesoproterozoic island arc in the southern Grenville Orogen, Llano uplift, central Texas: *Tectonophysics*, v. 265, p. 29-52.

Rose, P.R., 1972, Edwards Group, surface and subsurface, central Texas: University of Texas, Bureau of Economic Geology Report of Investigations 74, 198 p.

- Schindel, G. M. (2019). Genesis of the Edwards (Balcones Fault Zone) Aquifer. In *The Edwards Aquifer: The Past, Present, and Future of a Vital Water Resource*. Geological Society of America. [https://doi.org/10.1130/2019.1215\(02\)](https://doi.org/10.1130/2019.1215(02))
- Taggart, J. E., & Brookins, D. G. (1975). Rb-Sr whole rock age determinations for Sandia granite and Cibola gneiss. New Mexico: Isochron/West.
- Weeks, A. W. (1945). Balcones, Luling, and Mexia Fault Zones in Texas. *AAPG Bulletin*, 29. <https://doi.org/10.1306/3D9337B0-16B1-11D7-8645000102C1865D>
- Van der Hoven, S. J., & Quade, J. (2002). Tracing spatial and temporal variations in the sources of calcium in pedogenic carbonates in a semiarid environment. *Geoderma*, 108(3-4), 259-276.
- Young, B. W., & Chan, M. A. (2017). Gypsum veins in Triassic Moenkopi mudrocks of southern UT: Analogs to calcium sulphate veins on Mars. *Journal of Geophysical Research: Planets*, 122, 150-171. <https://doi.org/10.1002/2016JE005118>.

VITA

Hao Pham earned his Bachelor of Science in Geological Sciences from the University of Texas at El Paso in December 2020. With a keen passion for structural geology, he previously worked with Dr. Jason Ricketts by collecting over 300 veins orientation from Franklin Mountain in El Paso, TX. He has also assisted Dr. Lin Ma and Dr. Jason Ricketts in collecting water samples in central and southeast Texas for a major NSF Project researching riverine $^{234}\text{U}/^{238}\text{U}$ ratios in the entire state of Texas.

In Spring 2022, after being admitted to the master's program in Geological Sciences at the University of Texas at El Paso under the Department of Earth, Environmental, and Resources Sciences (DEERS), he found himself in a crossroad between studying structural geology and water geochemistry, thus in the end, he combined both studies into one project that would both satisfy the master's program and contribute to the NSF Project which resulted in this thesis.

Contact Information: Skypham09@gmail.com